JCI The Journal of Clinical Investigation

SLC44A2 regulates vascular smooth muscle cell phenotypic switching and aortic aneurysm

Tianyu Song, … , Liping Xie, Yong Ji

J Clin Invest. 2024. https://doi.org/10.1172/JCI173690.

Research In-Press Preview Vascular biology

Graphical abstract

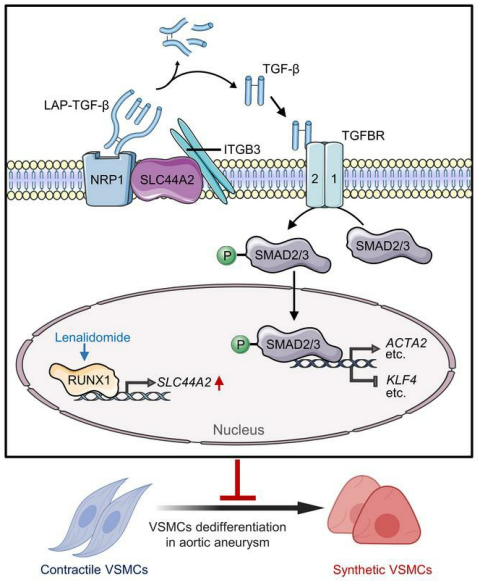

SLC44A2 regulates vascular smooth muscle cell phenotypic switching and aortic aneurysm

Authors

Tianyu Song[1,#]; Shuang Zhao[1,#]; Shanshan Luo[1,#]; Chuansheng Chen[1]; Xingeng Liu[1]; Xiaoqi Wu[1]; Zhongxu Sun[1]; Jiawei Cao[1]; Ziyu Wang[1]; Yineng Wang[1]; Bo Yu[2]; Zhiren Zhang[2,3]; Xiaolong Du[4]; Xiaoqiang Li[4]; Zhijian Han[5]; Hongshan Chen[1]; Feng Chen[6]; Liansheng Wang[7]; Hong Wang[8]; Kangyun Sun[9]; Yi Han[10,*]; Liping Xie[1,*]; Yong Ji[1,2,*].

Affiliations

[1]Gusu School, Nanjing Medical University, Suzhou, China; Key Laboratory of Cardiovascular and Cerebrovascular Medicine; Key Laboratory of Targeted Intervention of Cardiovascular Disease; Collaborative Innovation Center for Cardiovascular Disease Translational Medicine, Nanjing Medical University, Nanjing, Jiangsu, China;

[2]State Key Laboratory of Frigid Zone Cardiovascular Diseases (SKLFZCD), Harbin Medical University, Harbin, Heilongjiang, PR China;

[3]Departments of Cardiology, Central Laboratory, The First Affiliated Hospital of Harbin Medical University, NHC Key Laboratory of Cell Transplantation, Harbin Medical University, PR China;

[4]Department of Vascular Surgery, The Affiliated Nanjing Drum Tower Hospital, Nanjing University Medical School, Nanjing, China;

[5]Department of Urology, First Affiliated Hospital of Nanjing Medical University, Nanjing, China;

[6]Department of Forensic Medicine, Nanjing Medical University, Nanjing, China;

[7]Department of Cardiology, the First Affiliated Hospital of Nanjing Medical University, Nanjing Medical University, Nanjing, China;

[8]Center for Metabolic Disease Research, Department of Microbiology and Immunology, Temple University Lewis Katz School of Medicine, Philadelphia, PA, United States;

[9]Department of Cardiology, The Affiliated Suzhou Hospital of Nanjing Medical University, Suzhou Municipal Hospital, Gusu School, Nanjing Medical University, Suzhou, China;

[10]Critical Care Department, The Second Affiliated Hospital of Harbin Medical University, Harbin, Heilongjiang, PR China.

[#] These authors contributed equally

***Corresponding author:**

*Yong Ji, MD, PhD.

Gusu School, Nanjing Medical University, Suzhou, China; Key Laboratory of Cardiovascular and Cerebrovascular Medicine; Key Laboratory of Targeted

Intervention of Cardiovascular Disease; Collaborative Innovation Center for Cardiovascular Disease Translational Medicine, Nanjing Medical University, 101 Longmian Ave, Jiangning District, Nanjing, Jiangsu, 211166, China.
State Key Laboratory of Frigid Zone Cardiovascular Diseases (SKLFZCD), Harbin Medical University, 157 Baojian Rd, Nangang District, Harbin, Heilongjiang, 150081, China.
Tel: +86-451-86669473
E-mail: yongji@njmu.edu.cn; yongji@hrbmu.edu.cn

*Liping Xie, MD, PhD.
Gusu School, Nanjing Medical University, Suzhou, China; Key Laboratory of Cardiovascular and Cerebrovascular Medicine; Key Laboratory of Targeted Intervention of Cardiovascular Disease; Collaborative Innovation Center for Cardiovascular Disease Translational Medicine, Nanjing Medical University, 101 Longmian Ave, Jiangning District, Nanjing, Jiangsu, 211166, China.
Tel: +86-25-86869331
E-mail: lipingxie@njmu.edu.cn

*Yi Han, MD, PhD.
Critical Care Department, The Second Affiliated Hospital of Harbin Medical University, 246 Xuefu Rd, Nangang District, Harbin, Heilongjiang, 150086, China.
Tel: +86-451-86605052
E-mail: yihan@hrbmu.edu.cn; hanyi@jsph.org.cn

Conflict of interest: The authors have declared that no conflict of interest exists.

Abstract

Aortic aneurysm is a life-threatening disease with limited interventions, closely related to vascular smooth muscle cells (VSMCs) phenotypic switching. SLC44A2, a member of solute carrier series 44 (SLC44) family, remains under-characterized in the context of cardiovascular diseases. Venn diagram analysis based on microarray and single-cell RNA sequencing identified SLC44A2 as a major regulator of VSMCs phenotypic switching in aortic aneurysm. Screening for *Slc44a2* amongst aortic cell lineages demonstrated its predominant location in VSMCs. Elevated levels of SLC44A2 were evidenced in the aorta of both abdominal aortic aneurysm patients and angiotensin II (Ang II)-infused *Apoe*$^{-/-}$ mice. In vitro, SLC44A2 silencing promoted VSMCs towards a synthetic phenotype, while SLC44A2 overexpression attenuated VSMCs phenotypic switching. VSMCs-specific SLC44A2 knockout mice were more susceptible to aortic aneurysm under Ang II infusion, while SLC44A2 overexpression showed protective effects. Mechanistically, SLC44A2 interaction with NRP1 and ITGB3 activates TGF-β/SMAD signaling, thereby promoting contractile genes expression. Elevated SLC44A2 in aortic aneurysm is associated with upregulated runt-related transcription factor 1 (RUNX1). Furthermore, low dose of lenalidomide (LEN) suppressed aortic aneurysm progression by enhancing SLC44A2 expression. These findings reveal SLC44A2/NRP1/ITGB3 complex is a major regulator of VSMCs phenotypic switching and provide potential therapeutic approach (LEN) for aortic aneurysm treatment.

Introduction

Aortic aneurysm is defined as a localized enlargement of the aorta by at least 50% compared to the expected diameter in age-matched and sex-matched healthy individuals (1). Patients with aortic aneurysm typically remain asymptomatic until catastrophic complications like aortic rupture or dissection occur (2). Currently, therapeutic options for aortic aneurysm are limited to surgical interventions, with a lack of established pharmacological treatments to inhibit the aneurysm's progressive growth or prevent rupture (3). Thus, elucidating the regulatory mechanisms driving aortic aneurysm formation is essential for developing novel medical therapies.

Vascular smooth muscle cells (VSMCs) are critical to maintaining the vasoconstriction and vasodilatation of healthy vessels, exhibiting remarkable plasticity in response to environmental cues (4). Under pathological conditions, contractile VSMCs can dedifferentiate into a synthetic phenotype to produce elastolytic and proinflammatory factors, a process termed phenotypic switching (5). This switching contributes to extracellular matrix degradation, vascular inflammation, cell migration, and apoptosis, which are responsible for occurrence and aggravation of aortic aneurysm (6). Therefore, seeking the key nodes in VSMCs phenotypic switching may provide potential targets for aortic aneurysm management.

SLC44A2 belongs to the solute carrier series 44 (SLC44) family and was discovered as a supporting cell antigen in the inner ear (7). *Slc44a2*$^{-/-}$ mice show hair cell death and hearing loss (8). Recent studies have linked *SLC44A2* single nucleotide polymorphism (SNP) loci with venous thrombosis and Meniere's disease (9, 10).

However, the role of SLC44A2 in cardiovascular system remains undefined. Here we report SLC44A2 as a key regulator for VSMCs phenotypic switching, participating in the progression of aortic aneurysm. SLC44A2 interacts with neuropilin-1 (NRP1) to activate transforming growth factor β (TGF-β) signaling in an integrin β3 (ITGB3)-dependent manner, which maintains VSMCs contractile phenotype and alleviates aortic aneurysm. Additionally, lenalidomide (LEN) administration enhances SLC44A2 expression primarily through runt-related transcription factor 1 (RUNX1), leading to improvements in aortic aneurysm conditions, which provides a potential new therapeutic strategy for aortic aneurysm.

Results

Increased SLC44A2 in VSMCs is associated with aortic aneurysm.

To identify the candidate genes potentially related to VSMCs phenotypic switching in aortic aneurysm, we initially analyzed two datasets, VSMCs phenotype-related genes (11) and differentially expressed markers for VSMCs (12), to screen critical genes that are both involved in VSMCs phenotypic switching and highly expressed in VSMCs. Next, using the Gene Expression Omnibus database, we gathered differentially expressed genes (DEGs) in Human aortic aneurysm (GSE47472) and DEGs in VSMCs niched in Mouse aortic aneurysm (GSE186865) to uncover aortic aneurysm-relevant transcriptional signatures. As shown by Venn diagram, *SLC44A2*, *UCHL1*, *DKK3*, *ANXA3*, and *CRYAB* were overlapped from the aforementioned four datasets and emerged as main candidate genes linking VSMCs phenotypic switching to aortic aneurysm **(Figure 1A)**. We then detected these five genes in primary mouse aortic smooth muscle cells (MASMCs) from the whole aortas of saline-infused mice or angiotensin II (Ang II)-infused aortic aneurysm mouse models via quantitative real-time polymerase chain reaction (qRT-PCR), and found that SLC44A2 showed the most abundant and increased with highest fold change in MASMCs from Ang II-infused *Apoe*$^{-/-}$ mice **(Supplemental Figure 1A)**. Consistent results were also observed in MASMCs isolated from the whole abdominal aortas **(Figure 1B and Supplemental Figure 1B)**. Taken together, these results directed our focus towards the functional role of SLC44A2 in aortic aneurysm.

To generate a vista of SLC44A2 abundance amongst cell lineages niched within

the vascular wall, we reanalyzed single-cell RNA sequencing (scRNA-seq) data set of murine abdominal aortas (12). After applying integrative cell clustering analysis, results were visualized as a UMAP plot **(Figure 1C)**. Screening across eight major lineages demonstrated predominant SLC44A2 accumulation in VSMCs **(Figure 1D)**. Meanwhile, immunostaining of suprarenal abdominal aortas showed an elevation of SLC44A2 expression in Ang II-infused mice, coincided with reduced ACTA2 expression, an indicator of medial degeneration **(Figure 1E)**. The SLC44A2 mRNA level was also elevated in aortas from Ang II-infused mice **(Figure 1F)**. Importantly, we further verified that SLC44A2 protein and mRNA levels were significantly increased in patients with abdominal aortic aneurysm (AAA) **(Figure 1, G and H)**, with immunostaining indicating higher SLC44A2 levels in the media layer of human AAA aortas compared to controls **(Figure 1I)**. In vitro, SLC44A2 was increased after Ang II treatment in human aortic smooth muscle cells (HASMCs) at 6 hours and reached a peak at 24 hours **(Supplemental Figure 1C)**. These results suggest that upregulation of SLC44A2 in VSMCs may be involved in the progression of aortic aneurysm.

SLC44A2 modulates VSMCs phenotypic switching.

VSMCs demonstrate marked phenotypic modulation, ranging from a contractile state in quiescent mature arteries to a proliferative and synthetic state in aortic aneurysm. To investigate the role of elevated SLC44A2 in VSMCs phenotypic switching, we first tried to assess VSMCs phenotype by SLC44A2 knockdown. However, SLC44A2

165 silencing led to further increased VSMCs synthetic markers (OPN and KLF4) induced
166 by Ang II and repressed contractile markers (ACTA2 and TAGLN) **(Figure 2A)**. Cell-
167 embedded collagen gel contraction assay showed that SLC44A2 knockdown reduced
168 HASMCs contractility **(Figure 2B)**. Ang II-induced matrix metalloproteinase (MMP)
169 activation was further enhanced by SLC44A2 knockdown, as shown by in situ
170 zymography **(Figure 2C)** and gel zymography **(Figure 2D)**. Conversely, SLC44A2
171 overexpression could ameliorate Ang II-induced VSMCs phenotypic switching **(Figure**
172 **2E)**. HASMCs with SLC44A2 overexpression exhibited higher contractile capacity
173 **(Figure 2F)** and a reduction in MMP activities **(Figure 2, G and H)**. These findings
174 suggest that increased SLC44A2, as a compensatory mechanism, during aortic
175 aneurysm progression may play a protective role in maintaining the contractile
176 phenotype of VSMCs.

177 To further elucidate the role of SLC44A2 in VSMCs phenotypic switching, we
178 reintroduced SLC44A2 in SLC44A2-knockdown HASMCs. The result showed that
179 SLC44A2 re-expression reversed the increased synthetic markers and decreased
180 contractile markers induced by SLC44A2 knockdown **(Supplemental Figure 2A)**.
181 Meanwhile, SLC44A2 overexpression mitigated the aggravated MMP activity caused
182 by SLC44A2 knockdown **(Supplemental Figure 2B)**. These results suggested that
183 overexpression of SLC44A2 can counterbalance the effects of its knockdown, thereby
184 rescuing VSMCs from phenotypic switching. Next, we isolated primary MASMCs
185 from WT and *Slc44a2*^{KO} mice to evaluate the effect of SLC44A2 on phenotypic
186 switching in mouse-derived cells. Compared with WT MASMCs, *Slc44a2*^{KO} mouse-

derived MASMCs exhibited higher synthetic markers and lower contractile markers upon Ang II stimulation, which were reversed by SLC44A2 overexpression **(Supplemental Figure 2C)**. Additionally, SLC44A2 overexpression in WT MASMCs could alleviate Ang II-induced VSMCs phenotypic switching **(Supplemental Figure 2D)**. It demonstrates the vital function of SLC44A2 in preserving the contractile phenotype of VSMCs.

VSMCs specific SLC44A2 overexpression ameliorates Ang II-induced aortic aneurysm.

To delineate the function of SLC44A2 in VSMCs during aortic aneurysm, *Apoe*$^{-/-}$*/Tagln*$^{Cre/+}$ mice were intravenously injected with lentivirus carrying empty vector (Lenti-Vector) or SLC44A2 overexpression plasmid (Lenti-*Slc44a2*) containing 2 Loxp sites which can be recognized by Cre recombinase in VSMCs, facilitating SLC44A2 transcription **(Figure 3A)**. SLC44A2 overexpression in the tunica media was verified by immunostaining **(Supplemental Figure 3A)**. Body weight remained consistent across all groups **(Supplemental Figure 3B)**, and blood pressure increased similarly upon Ang II infusion in both Lenti-Vector and Lenti-*Slc44a2* mice **(Figure 3B)**. Strikingly, SLC44A2 overexpression in VSMCs blunted aortic aneurysm incidence induced by Ang II **(Figure 3C)**. In the presence of Ang II, mice developed aortic dilations and aneurysms, which was mitigated in Lenti-*Slc44a2* mice **(Figure 3D)**. The aortic rupture rate in Lenti-Vector mice was 27.27%, while that was 9.09% in Lenti-*Slc44a2* mice after Ang II infusion **(Supplemental Figure 3C)**. To quantify the dilation

of aortic aneurysm, we performed ultrasound imaging every 14 days to follow the changes in aortic diameter. Compared with the Lenti-Vector group, SLC44A2 overexpression inhibited aortic enlargement at 14 days and 28 days post-infusion of Ang II **(Supplemental Figure 3D and Figure 3E)**. Elastin damage is preferentially associated with progressive aortic dilatation. Notably, electron microscopic analysis revealed that the severe disruption of elastin fibers typically induced by Ang II was substantially mitigated in the aortas of Lenti-*Slc44a2* mice **(Figure 3F)**. Hematoxylin eosin (HE) staining indicated alleviated aortic dilatation in Lenti-*Slc44a2* mice in response to Ang II. Concomitantly, Elastic van Gieson (EVG) staining of aortic sections from Lenti-*Slc44a2* mice showed reduced media degeneration **(Figure 3G)**. An association of increased MMP activity with aortic aneurysm is well documented, where MMP promotes matrix degradation and impairs the integrity of the arterial wall. MMP activities, assessed by in situ zymography, were decreased in Lenti-*Slc44a2* mice after Ang II treatment **(Figure 3H)**. The suprarenal abdominal aorta from Ang II-infused mice displayed reduced expression of contractile marker (ACTA2) and elevated expression of synthetic marker (OPN) in VSMCs, indicating VSMCs dedifferentiation. In contrast, this dedifferentiation was inhibited in Lenti-*Slc44a2* mice **(Figure 3I)**. qRT-PCR assay also indicated that SLC44A2 overexpression restored contractile transcript levels and inhibited synthetic markers in aortas from Ang II-infused mice (**Supplemental Figure 3E**). Taken together, these findings prove that SLC44A2 suppresses Ang II-induced medial degeneration and restores the integrity of arterial wall, thus protecting against aortic aneurysm.

VSMCs specific SLC44A2 deficiency aggravates the development of Ang II-induced aortic aneurysm.

Besides gain-of-function, a loss-of-function approach was undertaken using mice lacking SLC44A2 in VSMCs (*Slc44a2*^{SMKO}) **(Figure 4A)**. Successful ablation of SLC44A2 was demonstrated by SLC44A2 detection **(Supplemental Figure 4A)**. Body weight and systolic blood pressure were comparable between the *Slc44a2*^{WT} and *Slc44a2*^{SMKO} groups **(Supplemental Figure 4B and Figure 4B)**. As expected, aortic aneurysm incidence was much higher in Ang II-infused *Slc44a2*^{SMKO} mice **(Figure 4C)**. SLC44A2 deficient mice were susceptible to aortic dilation and exhibited severe aneurysm **(Figure 4D)**. The aortic rupture rate was 25% in Ang II-infused *Slc44a2*^{SMKO} mice, while none rupture was recorded in *Slc44a2*^{WT} mice **(Supplemental Figure 4C)**. In vivo ultrasound showed that *Slc44a2*^{SMKO} mice exhibited larger maximal internal diameters than WT in response to Ang II **(Figure 4E)**. Additionally, the suprarenal abdominal aortas of *Slc44a2*^{SMKO} mice that received Ang II were characterized by more severe disruption of medial architecture with prominent elastin degradation **(Figure 4, F and G)**. Importantly, marked enhanced MMP activities were seen in suprarenal abdominal aortas of *Slc44a2*^{SMKO} mice **(Figure 4H)**. Immunofluorescence, qRT-PCR, and Western blot analysis of aortic tissue from *Slc44a2*^{SMKO} mice revealed a shift in VSMCs towards a synthetic phenotype **(Figure 4I, and Supplemental Figure 4, D and E)**. These data substantiate that VSMCs specific SLC44A2 deficiency accelerates the development and severity of aortic aneurysm.

Furthermore, we observed that the SLC44A2 deficiency induced VSMCs phenotypic switching, evidenced by significantly reduced ACTA2 expression, increased OPN expression, and enhanced MMP activity, occurred at 7 days after Ang II infusion, which is before the appearance of overt pathology **(Supplemental Figure 5, A-D)**. It suggested the compensatory effect of SLC44A2 on maintaining the contractile phenotype of VSMCs during the development of aortic aneurysm.

SLC44A2 preserves VSMCs contractile phenotype through the TGF-β/SMAD signaling via NRP1.

To investigate the potential mechanisms underlying SLC44A2-related VSMCs phenotypic switching, we performed co-immunoprecipitation assay combined with mass spectrometry to scan potential downstream effectors. We showed that SLC44A2 could interact with several proteins related to the TGF-β signaling and displayed the most abundant interaction with NRP1 **(Figure 5A)**. TGF-β signaling plays a vital role in VSMCs reprogramming, where VSMCs-specific ablation of TGF-β signaling in *Apoe*$^{-/-}$ mice drives aneurysm formation (13). Though the enhanced TGF-β level was observed in both patients and mice with aortic aneurysm, direct evidence shows that blocking TGF-β by neutralizing antibody accelerated the development of aortic pathology in Ang II- or elastase- induced aortic aneurysm mouse model (14-16). And consistently TGF-β overexpression by endovascular gene therapy stabilized existing aortic aneurysms in a xenotransplantation model (17). Emerging scRNA-seq analysis further support the adaptive activation of TGF-β signaling in VSMCs accounts for

maintaining aortic homeostasis and preventing aortic aneurysm (18).

We next assessed the effect of SLC44A2/NRP1 interaction on TGF-β signaling. Co-immunoprecipitation assay demonstrated the interaction of SLC44A2 with NRP1 in HASMCs and Ang II stimulation enhanced their association **(Figure 5, B and C)**. Proximity ligation assay (PLA) reveals close association of proteins (< 40 nm), and foci of SLC44A2/NRP1 signals were increased within the vascular media of Ang II-treated *Apoe*$^{-/-}$ mice. The affinity of SLC44A2 and NRP1 was further heightened in Lenti-*Slc44a2* group **(Figure 5D)**. Given NRP1's role in LAP-TGF-β (the inactive membrane-bound latent form) activation (19), we explore whether SLC44A2 participates in the regulation of the TGF-β signaling by detecting the TGF-β level in the medium of HASMCs. Indeed, SLC44A2 overexpression could further increase the TGF-β concentration **(Supplemental Figure 6A)** and the level of p-SMAD2/3 upon Ang II treatment **(Supplemental Figure 6B)**. The nuclear translocation of SMAD2 was elevated by SLC44A2 overexpression in Ang II-treated HASMCs **(Supplemental Figure 6, C and D)**. The elevated serum TGF-β concentration and p-SMAD2 were further confirmed in Ang II-infused *Apoe*$^{-/-}$ mice by Lenti-*Slc44A2* infection **(Supplemental Figure 6, E and F)**. Inversely, SLC44A2 knockdown inhibited the elevated TGF-β level and p-SMAD2 triggered by Ang II **(Supplemental Figure 6, G and H)**.

To further verify the notion that the positive effect of SLC44A2 on TGF-β activation is dependent on NRP1, we silenced NRP1 and assessed the consequences caused by SLC44A2 overexpression. The result showed that NRP1 knockdown

297 inhibited SLC44A2-mediated increases in TGF-β and SMAD2/3 phosphorylation
298 **(Figure 5, E and F)**. Furthermore, SLC44A2 overexpression reduced the elevated
299 synthetic markers and restored the reduced contractile markers induced by Ang II, the
300 effect of which was abolished by NRP1 knockdown **(Figure 5G)**. The enhanced
301 contractility of VSMCs by SLC44A2 overexpression was also nullified after NRP1
302 silencing **(Figure 5H)**. Gel zymography and in situ zymography assay showed that
303 NRP1 knockdown eliminated the protective effect of SLC44A2 overexpression against
304 increased MMP activities triggered by Ang II **(Figure 5, I and J)**. Collectively, these
305 results demonstrate that the prevention of VSMC phenotypic switching by SLC44A2
306 is NRP1-dependent.
307
308 **VSMCs contractile phenotype depends on the SLC44A2/NRP1/ITGB3 complex.**
309 To better understand the underlying molecular mechanism, we constructed plasmids of
310 His-tagged WT-NRP1 ($NRP1^{WT}$) and CUB, b1/b2 or MAM domain deleted-NRP1
311 ($NRP1^{\Delta CUB}$, $NRP1^{\Delta b1/b2}$, $NRP1^{\Delta MAM}$). These plasmids were co-transfected with
312 plasmids of HA-tagged WT-SLC44A2 in HEK293 cells, and co-immunoprecipitation
313 assay showed that NRP1-MAM domain deletion inhibited the interaction of SLC44A2
314 with NRP1 **(Figure 6A)**. Meanwhile, we found that residues 505-659 deletion in
315 SLC44A2 limited the interaction of SLC44A2 with NRP1 **(Figure 6B)**. These results
316 suggest that the MAM domain of NRP1 and residues 505-659 of SLC44A2 mediate
317 their association. Then we expressed WT or three peptides deleted SLC44A2 in
318 *Slc44a2*^{KO} MASMCs to detect the TGF-β level. Strikingly, both residues 55-232 and

505-659 deletion decreased TGF-β concentration **(Figure 6C)**, suggesting the latent molecular mechanism for TGF-β activation. The arginine154 (R154) in residues 55-232 of SLC44A2 is crucial for its binding to ITGB3 (20), a protein known to facilitate the cleavage of LAP, thereby activating latent TGF-β (21). In addition, ITGB3 is highly expressed in blood vessels (22). We speculated that the residues 55-232 of SLC44A2 is essential for binding ITGB3 to mediate TGF-β activation. The binding of ITGB3 to SLC44A2 was confirmed by co-immunoprecipitation assay **(Supplemental Figure 7A)**, and the high affinity of SLC44A2 and ITGB3 was observed in the vascular media of Ang II-infused *Apoe*$^{-/-}$ mice by PLA **(Figure 6D)**. Meanwhile, the residues 55-232 deletion disrupted the association between SLC44A2 and ITGB3 **(Figure 6E)**. SLC44A2 is able to recognize and bind to chaperones containing the VWF-A domain (7, 23). We showed that the VWF-A domain deletion of ITGB3 inhibited the interaction of SLC44A2 and ITGB3 **(Supplemental Figure 7B)**. Furthermore, SLC44A2 deficiency in VSMCs disrupted the combination of NRP1 and ITGB3 in the suprarenal abdominal aorta infused by Ang II for 3, 7, and 28 days (**Supplemental Figure 7, C and D, and Figure 6F**). In vitro experiments consistently showed that SLC44A2 knockdown inhibited the interaction of NRP1 and ITGB3 **(Figure 6G and Supplemental Figure 7E)**, suggesting that SLC44A2 acts as a scaffold protein binding both ITGB3 and NRP1. This was validated by GST-pull down assay using GST-tagged SLC44A2 and lysates from HASMCs and MASMCs, confirming SLC44A2 interacts with NRP1 and ITGB3 in vitro **(Supplemental Figure 7, F and G)**.

To further substantiate our findings, we assessed the TGF-β/SMAD signaling after

ITGB3 silencing. We found that ITGB3 knockdown abolished the effect of SLC44A2 overexpression-induced increase in medium TGF-β concentration and p-SMAD2/3 level under Ang II treatment **(Figure 6, H and I)**. Meanwhile, the suppression of MMP activities and the inhibition of phenotypic switching caused by SLC44A2 overexpression were nullified after ITGB3 knockdown **(Figure 6, J and K)**. To confirm the dependence of SLC44A2's effect on TGF-β, we employed a TGF-β-neutralizing antibody. It showed that blocking TGF-β reversed the protective effects of SLC44A2 on MMP activation and VSMCs phenotypic switching upon Ang II treatment **(Supplemental Figure 8, A and B)**. These data collectively demonstrate the crucial role of SLC44A2 in maintaining VSMCs contractile phenotype by interacting with NRP1 and ITGB3 to activate the TGF-β signaling.

RUNX1 regulates SLC44A2 transcription.

To unravel the molecular basis of SLC44A2 upregulation in aortic aneurysm, we integrated the prediction of *SLC44A2* promoter-binding transcription factors with digital gene expression (DGE) analysis of aortic RNAs from human and murine aortic aneurysm samples. RUNX1 was selected by inter-section analysis on recruited mRNA expression profiles (GSE17901, GSE51229, and GSE7084) and identified as a core regulator of SLC44A2 **(Figure 7A)**. Treatment of HASMCs with RUNX1 siRNA resulted in a significant decrease in SLC44A2 levels **(Figure 7B)**, Notably, RUNX1 level was elevated in aortic samples from patients with AAA (**Figure 7, C and D**). Luciferase assays showed that RUNX1-dependent *SLC44A2* activation was maintained

upon transfection with luciferase vector containing the -500 bp to +100 bp sequence of the *SLC44A2* promoter (**Figure 7E**). Mutations in the predicted binding sites (-252 bp to -242 bp) completely abrogated the effect of RUNX1 on SLC44A2 promoter activation, indicating this region's significance in transcription induction by RUNX1 **(Figure 7E)**. Taken together, upregulation of RUNX1 in VSMCs accounts for the induction of SLC44A2 during aortic aneurysm.

To validate RUNX1's binding to the SLC44A2 promoter, we performed EMSA assay using nuclear extracts from HASMCs and synthesized biotin-labeled oligonucleotide encompassing RUNX1 bind sites on SLC44A2 promoter. The observed protein binding (lane 2) was competed out by unlabeled probe (lane 3), and the binding signal was blocked by RUNX1 antibody (lane 4) but not by control IgG (lane 5) **(Supplemental Figure 9A)**. ChIP assay was performed to pull down RUNX1 and followed by qRT-PCR to amplify sequences containing RUNX1 binding site (-252 -CAGCCTCAATA- -242) in HASMCs. The result showed the binding of RUNX1 and SLC44A2 promoter sequence under physiological condition, which was enhanced by Ang II treatment **(Supplemental Figure 9B)**. Notably, RUNX1 overexpression further promoted the binding of RUNX1 and SLC44A2 promoter sequence **(Supplemental Figure 9B)**. Furthermore, Western blot analysis showed that overexpressing RUNX1 significantly enhanced SLC44A2 expression in HASMCs **(Supplemental Figure 9C)**.

Parallel results were obtained in MASMCs by EMSA, ChIP, and Western blot assay **(Supplemental Figure 9, D-F)**. These results provide evidence that RUNX1 directly binds to SLC44A2 promoter to regulate its expression both in MASMCs and HASMCs.

Lenalidomide (LEN) may act as an effective activator of RUNX1 to enhance SLC44A2 expression, inhibiting VSMCs phenotypic switching.

We next investigated the role of RUNX1 in regulating VSMCs phenotypic switching. As shown in **Supplemental Figure 10, A-D**, RUNX1 knockdown exacerbated Ang II-induced VSMCs phenotypic switching, but this was prevented in RUNX1-overexpressed VSMCs. Lenalidomide (LEN), which has demonstrated clinical efficacy in multiple myeloma with striking activity in myelodysplastic syndrome (MDS), can upregulate RUNX1 in haematopoietic stem and progenitor cells (24). Since the SLC44A2 transcription is modulated by RUNX1, we next evaluated the effect of LEN on VSMCs phenotypic switching. We observed that both RUNX1 and SLC44A2 levels began to increase modestly following 5 μM of LEN stimulation and reached at sustainable higher level at concentrations of 10-40 μM **(Supplemental Figure 11A)**. Consistent with expectations, LEN upregulated SLC44A2 expression upon Ang II treatment **(Supplemental Figure 11B).** Notably, LEN-induced SLC44A2 expression was negated by RUNX1 knockdown **(Supplemental Figure 11C)**, indicating that RUNX1 may be one of the major factors involved in LEN's effect on SLC44A2 expression.

LEN treatment significantly alleviated Ang II-induced MMP activation and contractile phenotype loss, the effects of which was normalized by SLC44A2 knockdown **(Supplemental Figure 11, D-F)**. Meanwhile, LEN-promoted TGF-β secretion was blunted by SLC44A2 silencing **(Supplemental Figure 11G)**. The results

together suggest that LEN inhibits VSMCs phenotypic switching through inducing SLC44A2 expression.

Supplementation with LEN suppresses aortic aneurysm initiation.

To assess LEN's in vivo efficacy, we administrated LEN daily for 28 days in aortic aneurysm model induced by Ang II infusion **(Figure 8A)**. LEN did not overtly affect body weight **(Supplemental Figure 12A)** and systolic blood pressure **(Supplemental Figure 12B)**. As reported, the most common adverse reactions of LEN at high doses are haematological adverse reactions, including neutropenia, thrombocytopenia, and anaemia (25). We therefore examined the effects of LEN on in vivo hematopoiesis. Administration of LEN did not induce myelosuppression **(Supplemental Table 2)**, consistent with the prior work that LEN does not cause a decline in peripheral blood counts in wild-type mice (26). Additionally, LEN showed no side effect on metabolic parameters and hepatorenal function **(Supplemental Table 3)**. Compared with the vehicle group, LEN-treated mice exhibited lower aortic aneurysm incidence after Ang II infusion **(Figure 8B)**, along with attenuated aorta dilation **(Figure 8C)**. The aortic rupture rate in vehicle group was 27.27%, while that was 9.09% in LEN-treated mice after Ang II infusion **(Supplemental Figure 12C)**. Diameters of suprarenal abdominal aorta were progressively increased after Ang II infusion, whereas LEN treatment inhibited the enlargement of aorta **(Figure 8D)**. Accordingly, transmural medial breaks were improved in LEN-treated groups **(Figure 8, E and F)**, concomitant with the reduced MMP activities and the mitigated VSMCs dedifferentiation in aortic tissues

(Figure 8, G and H, and Supplemental Figure 12D). Of note, co-staining of ACTA2 and SLC44A2 showed a significant upregulated SLC44A2 level in the media layer after LEN administration **(Supplemental Figure 12E)**. PLA signals for SLC44A2/NRP1/ITGB3 association was increased after LEN administration **(Supplemental Figure 12, F and G)**. Moreover, we observed elevated serum TGF-β levels and increased aortic SMAD2 phosphorylation under LEN treatment **(Supplemental Figure 12, H and I)**. Taken together, these data demonstrate that LEN activates TGF-β/SMAD signaling via SLC44A2 to prevent aortic aneurysm.

Finally, to verify the specific mechanism of LEN in vivo, we administrated LEN in Ang II-infused *Slc44a2*^{SMKO} mice. The results showed that the protective effect of LEN was totally abolished by SLC44A2 deficiency, as evidenced by unimproved aortic aneurysm incidence, aortic diameter expansion, aortic rupture rate, elastin breakage, and MMP activation in Ang II-infused *Slc44a2*^{SMKO} mice treated with LEN **(Supplemental Figure 13, A-H)**. These results conclusively demonstrate the effect of LEN is dependent on SLC44A2.

Discussion

This study elucidates the critical role of SLC44A2 in regulating VSMCs phenotypic switching and its implication in aortic aneurysm development. First, SLC44A2 was adaptively augmented in aortic aneurysm lesions from humans and mice. Overexpression of SLC44A2 in VSMCs mitigated the vascular remodeling of aortic aneurysm, while VSMCs specific knockout of SLC44A2 aggravated the development of aortic aneurysm in Ang II-infused mice. Moreover, mechanistic studies revealed that SLC44A2 mediated the interaction of NRP1 and ITGB3. The formation of NRP1/SLC44A2/ITGB3 trimolecular complex contributed to the activation of TGF-β and the following TGF-β/SMAD pathway elicitation to maintain the contractile phenotype of VSMCs. Additionally, we demonstrated that transcription factor RUNX1 could bind to *SLC44A2* gene promoter to activate its transcription. Last, LEN may upregulate RUNX1 to increase SLC44A2 expression, ameliorating VSMCs phenotypic switching and protecting against aortic aneurysm **(Figure 9)**.

SLC44A2 deficiency has been associated with hair cell loss, spiral ganglion degeneration, and hearing loss in mice, and with Meniere disease and transfusion-related acute lung injury in humans (10, 23). Emerging data describe that SLC44A2 is a thrombosis regulator controlling mitochondrial energetics in platelet activation and production of neutrophil extracellular traps (20, 27). Genome-wide association studies have linked the expression of the human neutrophil antigen 3b epitope on the SLC44A2 protein with a 30% decreased risk of venous thrombosis (28). However, the precise role of SLC44A2 in cardiovascular disease is not well understood. Although SLC44A2 was

upregulated in aortic aneurysm tissues from humans and mice, we found a profound suppressive effect of SLC44A2 on aortic aneurysm development. Notably, SLC44A2 was markedly increased in Ang II-induced aneurysmal mice, in parallel with the activation of TGF-β signaling including TGF-β secretion and SMAD2/3 phosphorylation. Accumulating evidence highlights that upregulated TGF-β levels during aortic aneurysm may serve as an adaptive response to maintain aortic strength, and the blockade of TGF-β by neutralizing antibody could promote the development and rupture of aortic aneurysm in experimental aneurysm models (14, 16, 18). Similarly, a previous study documented that Ang II caused a significant rise in ADAM15 protein levels in the abdominal aorta, which could be an important compensatory mechanism that limits aortic aneurysm formation, whereas mice lacking ADAM15 developed aortic aneurysm (29). Another study reported that hepcidin expression was markedly raised in VSMCs within the aneurysm tissue, and mice with VSMCs-specific deletion of hepcidin exhibited a heightened phenotype of aortic aneurysm (30). We demonstrated here that enhanced SLC44A2 acts as an adaptive program in VSMCs that attenuates VSMCs dedifferentiation and protects against aortic aneurysm. By activating TGF-β signaling, SLC44A2 could effectively amplify the adaptive response in the aortic wall.

SLC44A2 mainly locates at cell membrane and mitochondrial membrane, and functions by interacting with proteins containing VWF-A domains. SLC44A2 was initially reported as an antigen in the inner ear, essential for maintaining normal hearing through its interaction with cochlin (7). Furthermore, SLC44A2 can bind to von

Willebrand factor (VWF), a key molecule in hemostasis, and this interaction on neutrophils leads to agglutination (23). Arg154Gln polymorphism of SLC44A2 results in a reduced binding of SLC44A2 to VWF (9). We identified NRP1 as a binding partner of SLC44A2 by mass spectrum scanning. NRP1 knockdown abolished the protective effect of SLC44A2 overexpression against VSMCs phenotypical switching. NRP1 is capable of binding to a broad repertoire of ligands, accounting for its diverse biological functions in immunity, tumorigenesis, and vascular development (31). NRP1 exerts pleiotropic roles in TGF-β signaling, where it activates TGF-β signaling in stromal fibroblast cell lines and breast cancer cells (32). Conversely, NRP1 suppresses the endothelial stalk-cell phenotype by limiting TGF-β/SMAD activation (33). NRP1 is a high-affinity receptor for inactive membrane-bound latent form, LAP-TGF-β in T cells (34), while the precise molecular mechanism underlying NRP1-induced latent TGF-β activation remains unclear.

It is well established that LAP-TGF-β activation occurs in an integrins-dependent manner (21). Integrins bind to arginine-glycine-aspartic acid (RGD) motif in the LAP segment, which leads to a physical traction/stress-mediated deformation of the latent complex, allowing for subsequent liberation of active TGF-β (35). Notably, integrin αvβ3 is abundant in blood vessels (22) and its regulation of Rho GTPase activation is involved in VSMCs differentiation (36). SLC44A2 engagement with ITGB3 mediates adhesion of neutrophils to primed platelets (20), but the interaction between SLC44A2 and ITGB3 in VSMCs is yet to be elucidated. Our results demonstrate that SLC44A2 acts as a scaffold protein, assembling ITGB3 and NRP1, thereby activating the TGF-

β/SMAD signaling pathway. We showed that the amino acid sequence 505-659 of SLC44A2 was essential for binding NRP1 with its MAM domain, while the amino acid sequence 55-232 of SLC44A2 was essential for binding ITGB3 with its VWF-A domain. These results provided the evidence for the regulatory SLC44A2/NRP1/ITGB3 signaling axis in TGF-β activation.

TGF-β signaling plays a vital but diverse role in aortic aneurysm and VSMCs reprogramming (37). Some literature posits that the activation TGF-β signaling in VSMCs is the primary cause of Marfan and Loeys-Dietz syndromes (38, 39), where these inherited aortic aneurysms predispositions were initially proposed to be due to overactivity in the TGF-β pathway. However, most current evidence supports the reverse hypothesis that the TGF-β pathway protects against aortic aneurysm formation (40, 41). Indeed, pathogenic variants or deficiency of TGF-β pathway genes including *TGFB2*, *TGFB3*, *TGFBR1*, *TGFBR2*, and *SMAD3*, confer risks for aortic destruction and thoracic aortic aneurysm formation (42). A combination of reduced TGF-β signaling and hypercholesterolemia drives ascending aortic aneurysm development (13). Meanwhile, anti-TGF-β blocking antibody has been used to augment aneurysm growth and induce intraluminal thrombus when establishing aortic aneurysm mouse model (43). This was in agreement with a single study showing that adenovirus-mediated overexpression of TGF-β stabilized expanding aortic aneurysm in rats (17). When overexpressed in the heart and plasma, TGF-β1 is a vasculoprotective cytokine that prevents aortic dilation (44). Additionally, intramural delivery of TGF-β1 hydrogel can effectively decrease aneurysm progression in $CaCl_2$-induced aortic aneurysm (45).

Proefferocytic anti-CD47 antibodies therapy promotes TGF-β signaling and prevents aneurysm formation (46). These evidences suggest that upregulating the TGF-β pathway is a legitimate therapeutic approach for aortic aneurysm, assuming effective and safe interventions can be developed.

TGF-β/SMAD signaling protects against aortic aneurysm by abrogation of VSMCs phenotypic switching. Mutations in TGFBR2 compromises both basal and TGF-β-induced expression of contractile proteins in VSMCs (47). Loss of smooth muscle TGF-β signaling input, when combined with hyperlipidemia, results in a transdifferentiation of small population of VSMCs to a mesenchymal stem cell-like state (13). Our results consistently reveal that SLC44A2 maintains VSMCs contractile genes transcription by activating TGF-β/SMAD signaling.

So far, the transcriptional regulation of SLC44A2 remains unclear. In our study, we identified RUNX1 as a regulator of SLC44A2 transcription. We found that the upregulated RUNX1 in VSMCs contributed to the compensating increase of SLC44A2 during aortic aneurysm. RUNX1 is a vital transcription factor in hematopoiesis and its dysregulation is intimately related to myelodysplastic syndrome (MDS) (48). Lenalidomide (LEN) is the first-line medication for MDS by reversing the cytologic and cytogenetic abnormalities by upregulating RUNX1 (24, 49). Our study indicated that RUNX1 may be one of the major factors involved in LEN effects on SLC44A2 expression. Use of LEN in vivo significantly reduced the incidence of aortic aneurysm. Moreover, compared with the dosage of LEN (50 mg/kg/day) for hematological disease (26), the application of low dose LEN (20 mg/kg/day) showed an effective role for

aortic aneurysm therapy in mice with no haematological adverse reactions including neutropenia, thrombocytopenia, and anaemia. This finding is consistent with thrombocytopenia seen in patients treated with LEN, which is often a dose-limiting toxicity (50, 51). Treatment with LEN may facilitate the clinical management of aortic aneurysm.

There are several limitations for this study. First, the long-axis ultrasonic imaging evaluates aortic diameter in the anterior-posterior direction and may result in underestimations of aortic diameter compared to short-axis measurement in both anterior-posterior and transverse directions (52). Second, MASMCs isolation from the whole abdominal aorta has a limited ability of exhibiting the specific features of aortic aneurysm, given that aortic dilation in Ang II-infused mice occurs predominantly in the suprarenal abdominal aorta. Also, our study found that SLC44A2 expression was increased in aortas of patients with abdominal aortic aneurysm (AAA), unveiling that SLC44A2 may be exploited as a promising target for therapy development against AAA. This direction deserves future confirmation studies using larger patient cohorts of AAA. Our results revealed that LEN suppressed aortic aneurysm initiation in Ang II-induced mouse models, highlighting LEN supplementation as a potential treatment for aortic aneurysm. Extending clinical research will be required to validate the efficacy and translational feasibility of LEN in AAA management. Finally, given the dose-limiting haematological adverse reactions of LEN, further studies are expected to elucidate the safety, tolerability, and pharmacokinetic profile in long-term clinical use for AAA.

In summary, we uncovered a crucial role of SLC44A2 in activating the TGF-β/SMAD signaling by interacting with NRP1 and ITGB3, which is essential for VSMCs contractile phenotype maintenance. LEN inhibits VSMCs phenotypic switching by modulating RUNX1/SLC44A2 axis and improves the aortic pathology in mouse aortic aneurysm models, revealing a potential prospect for clinical application in humans.

Methods

All supporting data are available within the article and Supplemental Methods. Detailed descriptions of experimental methods of the current study are provided in Supplemental Methods.

Sex as a biological variable

Our study exclusively examined male mice because aortic aneurysm is a sex dimorphic disease and aortic aneurysm exhibits lower female prevalence (1, 53). It is unknown whether the findings are relevant for female mice.

Single-cell RNA sequencing (scRNA-seq) and analysis

Analysis of scRNA-seq data was performed according to the previous literature (54). Cells with a mitochondria ratio >20% and <500 genes were filtered out. Integrative cell clustering results were visualized as a 2-dimensional UMAP plot and read counts were natural-log normalized (each transcript counts/total counts × 10000) using the "NormalizeData" function for each cell. Following single-cell clustering and annotation of each cell state cluster, we predominantly focused on *Slc44a2* expression pattern across eight-cell lineages, encompassing vascular smooth muscle cells, fibroblasts, endothelial cells, macrophages, T cells, B cells, erythrocyte cells, and dendritic cells. scRNA-seq data were available at the Gene Expression Omnibus (GEO) under the access number of GSE152583 (12).

Human tissue sample acquisition and preparation

The use of human aortic tissue was approved by the medical ethics committee of

Nanjing Drum Tower Hospital and the ethics committee of Nanjing Medical University following the Declaration of Helsinki. Two types of human abdominal aortic tissues were used for this study: abdominal aortic aneurysm (AAA) samples (n = 6) and non-AAA samples (n = 6). The diagnosis of AAA was confirmed by computed tomographic angiography. Abdominal aortic tissues were collected during surgical repair for AAA. Non-AAA samples were obtained from organ donor controls. Written informed consent was provided by all participants or the organ donors' legal representatives before enrollment.

As previously described (55-57), aorta segments were freshly isolated in the operating theatre, with AAA tissue harvested at the maximal dilation. The aortic tissue was then processed as follows. Both non-AAA and AAA aortic samples were placed in ice-cold physiological salt solution immediately upon removal, followed by stripped of the periaortic tissue and mural thrombus. The aortic tissue was divided into several segments, which were either fixed in 4% paraformaldehyde for histologic analyses or snap-frozen in liquid nitrogen followed by storage at -80°C for RNA or protein extraction. The entire process from aorta collection to tissue processing and storing was completed within 3 h.

Animal studies

Apoe$^{-/-}$ mice were purchased from GemPharmatech Co. Ltd. (Nanjing, China) and *Tagln*$^{Cre/+}$ mice were purchased from the Model Animal Research Center of Nanjing University. *Slc44a2*^{KO} and *Slc44a2*$^{flox/flox}$ mice were originally generated by the Animal Center of Nanjing Medical University. For specific ablation of SLC44A2 in vascular

626 smooth muscle cells (*Slc44a2*$^{SMKO)}$, *Slc44a2*$^{flox/flox}$ mice were crossed with *Tagln*$^{Cre/+}$
627 mice. *Apoe*$^{-/-}$ mice were crossed with *Tagln*$^{Cre/+}$ mice to generate *Apoe*$^{-/-}$/*Tagln*$^{Cre/+}$ mice.
628 PCR primers (5'-3') used for genotyping were as follows:
629 TCGCAGAATTACTACGGGAAGC; GGGTGACCAGCTGATTCATCAG
630 (*Slc44a2*$^{flox/flox}$ mice); TGCCACGACCAAGTGACAGCAATG;
631 ACCAGAGACGGAAATCCATCGCTC (*Tagln*$^{Cre/+}$ mice). All experimental male mice
632 (8 to 10 weeks old) were on a C57BL/6J background and maintained with free access
633 to chow food and water.

634 **Aortic aneurysm model**

635 Ang II-induced aneurysm model: 8- to 10-week-old male mice were infused with Ang
636 II (1,000 ng/kg/min) or saline by osmotic pumps (Alzet model 2004, Alza Corp) for 28
637 days. Mice were anesthetized with inhaled isoflurane and the minipumps were
638 surgically implanted into the subcutaneous space of the mice in the back of the neck.
639 Animals were regularly monitored and weighed. Aneurysm was defined as a ≥50%
640 increase in aortic diameter of the segment in unchallenged mice with the same genetic
641 background.

642 **Abdominal ultrasonography in mice**

643 Aortic diameters were measured by high-frequency ultrasound Vevo 2100 echography
644 device (VisualSonics). These measurements were performed on the day 0, day 14, and
645 day 28 after Ang II infusion. Mice were anesthetized using 2% isoflurane and placed
646 on a supine position. The abdominal area was shaved and coated with ultrasound

transmission gel before positioning the acquisition probe. As previously described (58-60), long-axis ultrasound scans of suprarenal aortas were performed from the aortic hiatus to the renal artery. The probe was first applied on the short axis to locate the abdominal aorta, adjacent to the inferior vena cava. The abdominal aorta was then centered and the probe was switched to the long axis. Color mode was activated to help localize the two renal arteries, displaying a red blood flow toward the probe on the screen. The probe was then adjusted to capture the area of the maximum dilation in the suprarenal abdominal aorta. Maximal internal diameters of aortic images were measured with the Vevo LAB software.

Lentivirus-mediated overexpression

Mouse Slc44a2 cDNA was amplified by PCR and cloned into the pLVX-FLEX-EF1a-ZsGreen lentiviral vector. The correct sequence of Slc44a2 gene in this construct was verified by sequencing. We cloned the expression cassette in an inverse, anti-sense orientation between two different loxP sites. The construct was designed so that Cre induction could be used to mediate the inversion of the Slc44a2 cassette into a sense orientation. Control or Slc44a2 lentivirus (10^9 TU per mouse) was injected into *Apoe*$^{-/-}$*/Tagln*$^{Cre/+}$ mice via tail vein. In these mice, Cre induction mediated the initial flipping of the cassette, contingent on the orientation and location of two loxP sites.

Drug administration

Stock solution of LEN was prepared in dimethyl sulfoxide (DMSO), stored at -80°C, and diluted with sterile saline before intragastrically administration. To examine its

preventive effects against Ang II-induced aortic aneurysm, *Apoe*$^{-/-}$ mice were administered LEN via oral gavage concurrent with the 28-day Ang II infusion period.

Transmission electron microscopy

Suprarenal abdominal aortas were dissected and sliced into small fragments of 3-5 mm each. Aorta slices were then fixed in 5% glutaraldehyde for 1-2 days. Specimens were post-fixed in 1% osmium tetroxide. After *en bloc* staining with 2% aqueous uranyl acetate for 2 h, samples were dehydrated in series of ethanol up to 100% and embedded in epoxy resin. Ultrathin sections were cut with an EM UC7 ultramicrotome (Leica) and poststained with lead nitrate. Sample grids were observed under JEM-1400Flash Electron Microscope (JEOL).

MMP activity determined by in situ zymography and gel zymography

For in situ zymography, MMP activity was determined by a EnzChek™ Gelatinase/Collagenase assay kit (#E12055, Thermo Fisher Scientific) following the manufacturer's protocol. The isolated suprarenal abdominal aortic tissue was embedded into OCT solution and rapidly frozen with dry ice. Freshly cut frozen aortic sections or HASMCs were incubated with a fluorogenic gelatin substrate (DQ gelatin) at a concentration of 25 μg/mL at 37℃ for 24 h, while being protected from light. The fluorescence of DQ gelatin is quenched until MMP-catalyzed hydrolysis occurs. The resulting fluorescence intensity is directly proportional to proteolytic digestion. Negative control zymograms were incubated in the presence of the MMP inhibitor (1,10-phenanthroline, 10 mM). The samples were then fixed in 4% PFA and stained

with DAPI. Proteolytic activity was detected as green fluorescence (at 495 nm absorption/515 nm emission) by confocal microscopy (Zeiss LSM 800).

For gel zymography, supernatants from cultured HASMCs were harvested and centrifuged by Amicon Ultra Centrifugal Filter (#UFC801096, Millipore) to yield concentrated conditioned media, as previously described (61). The conditioned media were then subjected to 10% sodium dodecyl sulfate polyacrylamide gel electrophoresis (SDS-PAGE) polymerized in the presence of 1 mg/mL gelatin as a substrate for MMP activity. After electrophoresis, gels were washed three times by 2.5% Triton X-100 to remove SDS, and then incubated for 48 h (37℃) in developing buffer (50 mM Tris-HCl (pH 7.4), 150 mM NaCl, 5 mM $CaCl_2$, and 0.1% Brij-35). The gels were then stained with Coomassie Brilliant Blue and destained to reveal clear bands indicating zones of gelatinolytic activity.

Proximity ligation assay (PLA)

PLA was performed with Duolink reagents (#DUO92101, Sigma) following the manufacturer's instructions. Suprarenal abdominal aortic cryosections or cells were fixed with 4% PFA and permeabilized in the same manner as the standard immunostaining procedure (62), followed by blocked with Duolink blocking buffer for 1 h. Primary antibodies from two different species were then incubated overnight at 4˚C. After washing, exact PLUS and MINUS probes conjugated with secondary antibodies were added and hybridized for 1 h at 37℃. Ligation, rolling circle amplification, and detection with fluorescent probes were performed. PLA signals, recognized as red fluorescent dots, were visualized and images were captured using

confocal microscopy (Zeiss LSM 800). The primary antibodies used were mouse anti-SLC44A2 (#sc-101266, Santa Cruz Biotechnology), rabbit anti-NRP1 (#ab81321, Abcam), mouse anti-NRP1 (#sc-5307, Santa Cruz Biotechnology), and rabbit anti-ITGB3 (#18309, Proteintech). Negative controls were performed using only one primary antibody.

Cell culture

HASMCs (#6110, Sciencell) were propagated in smooth muscle cell medium (#1101, Sciencell) with 2% fetal bovine serum (FBS), Smooth Muscle Cell Growth Supplement (SMCGS), and 100 U/mL p/s at 37℃ with 5% CO_2.

HEK293 cells purchased from American Type Culture Collection were maintained in Dulbecco's modified Eagle's medium (DMEM, Thermo Fisher Scientific) or DMEM/F12 (Thermo Fisher Scientific) with 10% FBS (Gibco).

Confluent cells (80-85%) were rested in serum-free cultured medium for 24 h and treated with Ang II (1 μM) at the specified times, followed by subsequent experiments (transfection, etc.).

Isolation of MASMCs

MASMCs were isolated from the whole aortas or the whole abdominal aortas of saline-infused mice or Ang II-infused aortic aneurysm mouse models by enzymatic digestion as described before (63, 64). Briefly, mice were dissected until the thoracic cavity was exposed, then perfused with cold sterile PBS. The aorta was cleaned from surrounding tissues, followed by rinsing the aorta in cold sterile PBS. Then adventitia and

endothelium were gently removed, and the aorta was cut into 1-2 mm explants. The finely cut tissues were digested in collagenase type II (#LS004177, Worthington Biochemical Corporation) at 37℃ with 5% CO_2 in the incubator for 3-4 h. Afterwards, same amount of FBS was added to stop the enzymatic reaction. Cell pellet was collected by centrifuged at 2,000 g for 10 min and supernatant was discarded as much as possible. Cells were resuspended with DMEM supplemented with 10% FBS and 100 U/mL p/s. MASMCs were identified based on immunofluorescent staining of ACTA2.

Collagen gel contraction assay

HASMCs were treated with siRNA or lentivirus and cultured in serum-free cultured medium for 24 h prior to being seeded into collagen gels as previously described (65). Collagen gels were prepared by mixing HASMCs with type I collagen (#A1048301, Thermo Fisher Scientific), 2 × DMEM, 1 M NaOH, and distilled water. The mixture was seeded in 24-well cell culture plates and incubated in 37℃ for 30 min. Polymerized gels were then dislodged from the well by gentle mechanical force. Digital photographs of collagen gel lattices were taken after 24 h, and the gel surface area was measured by Image J.

Statistical analysis

All values are presented in the figures as mean ± SEM with $P<0.05$ considered statistically significant. The *n* numbers in figure legends represent biological replicates or the number of mice and human samples. For statistical comparisons, we first evaluated whether data were normally distributed using Shapiro-Wilk normality test.

Nonparametric tests were used when data were not normally distributed. For two-group parametric tests, the Levene test was applied to assess the equality of variances. Significant difference between two groups was determined by unpaired, two-tailed Student's *t* test when data showed equal variance; otherwise, *t* test assuming unequal variance was performed. For comparisons among more than 2 groups, Brown-Forsythe test was used to evaluate homogeneity of variance. For comparing the differences between different groups, one-way ANOVA or Welch ANOVA was applied for equal variances assumed or not, respectively. Two-way ANOVA with mixed-effects was used for comparing the parameters that were repeatedly measured over time, including body weight, blood pressure, and inner diameters of suprarenal abdominal aorta of the mice at 0 to 28 days after osmotic pumps implantation. All graphs and statistical analyses were performed by GraphPad Prism 8.

Study approval

The use of human aortic tissue was approved by the medical ethics committee of Nanjing Drum Tower Hospital and the ethics committee of Nanjing Medical University following the Declaration of Helsinki. Written informed consent was provided by all participants or the organ donors' legal representatives before enrollment. All animal experiments were conducted in accordance with the ARRIVE guidelines for the care and use of laboratory animals, and with approval of the Nanjing Medical University Animal Care and Use Committee.

Data availability

774 Values for all data points in graphs are reported in the Supporting Data Values file.

775

Author Contributions

Y.J., L.X., and Y.H. developed the concept, designed the study, and revised the manuscript. T.S. and S.Z. analysed the data and drafted the manuscript. T.S., S.Z., S.L., and C.C. performed the experiments. X.L., X.W., J.C., Z.W., and Y.W. provided technical assistance. Z.S. re-analysed RNA sequencing datasets. X.D. and X.L. provided clinical samples. Z.H., H.C., F.C., L.W., H.W., K.S., B.Y., and Z.Z. supervised the in vivo and in vitro study. The order of co-first authors was determined by the volume of work each contributed to the study.

Acknowledgements

This work was supported by grants from the National Natural Science Foundation of China (grant NOs. 82121001, 82241211, 82030013, 82070278, 82100414, 82370262, 82070475, 81820108002, 82222009), the National Key Research and Development Program of China (2019YFA0802704), and the Young Elite Scientists Sponsorship Program by China Association for Science and Technology (YESS20220214). The authors thank Dr. Jingjing Ben (Department of Pathophysiology, Nanjing Medical University, Nanjing, China) for sharing pLVX-FLEX-EF1a-ZsGreen plasmid.

References

1. Bossone E, and Eagle KA. Epidemiology and management of aortic disease: aortic aneurysms and acute aortic syndromes. *Nat Rev Cardiol.* 2021;18(5):331-348.
2. Pinard A, et al. Genetics of Thoracic and Abdominal Aortic Diseases. *Circ Res.* 2019;124(4):588-606.
3. Golledge J. Abdominal aortic aneurysm: update on pathogenesis and medical treatments. *Nat Rev Cardiol.* 2019;16(4):225-242.
4. Chakraborty R, et al. Histone Acetyltransferases p300 and CBP Coordinate Distinct Chromatin Remodeling Programs in Vascular Smooth Muscle Plasticity. *Circulation.* 2022;145(23):1720-1737.
5. Cai D, et al. A Novel Mechanism Underlying Inflammatory Smooth Muscle Phenotype in Abdominal Aortic Aneurysm. *Circ Res.* 2021;129(10):e202-e214.
6. Petsophonsakul P, et al. Role of Vascular Smooth Muscle Cell Phenotypic Switching and Calcification in Aortic Aneurysm Formation. *Arterioscler Thromb Vasc Biol.* 2019;39(7):1351-1368.
7. Kommareddi PK, et al. Cochlin isoforms and their interaction with CTL2 (SLC44A2) in the inner ear. *J Assoc Res Otolaryngol.* 2007;8(4):435-446.
8. Kommareddi P, et al. Hair Cell Loss, Spiral Ganglion Degeneration, and Progressive Sensorineural Hearing Loss in Mice with Targeted Deletion of Slc44a2/Ctl2. *J Assoc Res Otolaryngol.* 2015;16(6):695-712.
9. Zirka G, et al. Impaired adhesion of neutrophils expressing Slc44a2/HNA-3b to

VWF protects against NETosis under venous shear rates. *Blood.* 2021;137(16):2256-2266.

10. Nair TS, et al. SLC44A2 single nucleotide polymorphisms, isoforms, and expression: Association with severity of Meniere's disease? *Genomics.* 2016;108(5-6):201-208.

11. Jia Y, et al. PHB2 Maintains the Contractile Phenotype of VSMCs by Counteracting PKM2 Splicing. *Circ Res.* 2022;131(10):807-824.

12. Zhao G, et al. Single-cell RNA sequencing reveals the cellular heterogeneity of aneurysmal infrarenal abdominal aorta. *Cardiovasc Res.* 2021;117(5):1402-1416.

13. Chen PY, et al. Smooth Muscle Cell Reprogramming in Aortic Aneurysms. *Cell Stem Cell.* 2020;26(4):542-557 e511.

14. Wang Y, et al. TGF-beta activity protects against inflammatory aortic aneurysm progression and complications in angiotensin II-infused mice. *J Clin Invest.* 2010;120(2):422-432.

15. Angelov SN, et al. TGF-beta (Transforming Growth Factor-beta) Signaling Protects the Thoracic and Abdominal Aorta From Angiotensin II-Induced Pathology by Distinct Mechanisms. *Arterioscler Thromb Vasc Biol.* 2017;37(11):2102-2113.

16. Lareyre F, et al. TGFbeta (Transforming Growth Factor-beta) Blockade Induces a Human-Like Disease in a Nondissecting Mouse Model of Abdominal Aortic Aneurysm. *Arterioscler Thromb Vasc Biol.* 2017;37(11):2171-2181.

17. Dai J, et al. Overexpression of transforming growth factor-beta1 stabilizes already-formed aortic aneurysms: a first approach to induction of functional healing by endovascular gene therapy. *Circulation.* 2005;112(7):1008-1015.

18. Zhang C, et al. Aortic Stress Activates an Adaptive Program in Thoracic Aortic Smooth Muscle Cells That Maintains Aortic Strength and Protects Against Aneurysm and Dissection in Mice. *Arterioscler Thromb Vasc Biol.* 2023;43(2):234-252.

19. Chaudhary B, et al. Neuropilin 1: function and therapeutic potential in cancer. *Cancer Immunol Immunother.* 2014;63(2):81-99.

20. Constantinescu-Bercu A, et al. Activated alpha(IIb)beta(3) on platelets mediates flow-dependent NETosis via SLC44A2. *Elife.* 2020;9.

21. Budi EH, et al. Transforming Growth Factor-beta Receptors and Smads: Regulatory Complexity and Functional Versatility. *Trends Cell Biol.* 2017;27(9):658-672.

22. Xie Y, et al. LMO7 Is a Negative Feedback Regulator of Transforming Growth Factor beta Signaling and Fibrosis. *Circulation.* 2019;139(5):679-693.

23. Bayat B, et al. Choline Transporter-Like Protein-2: New von Willebrand Factor-Binding Partner Involved in Antibody-Mediated Neutrophil Activation and Transfusion-Related Acute Lung Injury. *Arterioscler Thromb Vasc Biol.* 2015;35(7):1616-1622.

24. Martinez-Hoyer S, et al. Loss of lenalidomide-induced megakaryocytic differentiation leads to therapy resistance in del(5q) myelodysplastic syndrome.

Nat Cell Biol. 2020;22(5):526-533.

25. Jackson GH, et al. Lenalidomide maintenance versus observation for patients with newly diagnosed multiple myeloma (Myeloma XI): a multicentre, open-label, randomised, phase 3 trial. *Lancet Oncol.* 2019;20(1):57-73.

26. Fink EC, et al. Crbn (I391V) is sufficient to confer in vivo sensitivity to thalidomide and its derivatives in mice. *Blood.* 2018;132(14):1535-1544.

27. Bennett JA, et al. The choline transporter Slc44a2 controls platelet activation and thrombosis by regulating mitochondrial function. *Nat Commun.* 2020;11(1):3479.

28. Germain M, et al. Meta-analysis of 65,734 individuals identifies TSPAN15 and SLC44A2 as two susceptibility loci for venous thromboembolism. *Am J Hum Genet.* 2015;96(4):532-542.

29. Jana S, et al. ADAM (a Disintegrin and Metalloproteinase) 15 Deficiency Exacerbates Ang II (Angiotensin II)-Induced Aortic Remodeling Leading to Abdominal Aortic Aneurysm. *Arterioscler Thromb Vasc Biol.* 2020;40(8):1918-1934.

30. Loick P, et al. Protective Role for Smooth Muscle Cell Hepcidin in Abdominal Aortic Aneurysm. *Arterioscler Thromb Vasc Biol.* 2023;43(5):713-725.

31. Chuckran CA, et al. Neuropilin-1: a checkpoint target with unique implications for cancer immunology and immunotherapy. *J Immunother Cancer.* 2020;8(2).

32. Vivekanandhan S, and Mukhopadhyay D. Genetic status of KRAS influences Transforming Growth Factor-beta (TGF-beta) signaling: An insight into

Neuropilin-1 (NRP1) mediated tumorigenesis. *Semin Cancer Biol.* 2019;54:72-79.

33. Aspalter IM, et al. Alk1 and Alk5 inhibition by Nrp1 controls vascular sprouting downstream of Notch. *Nat Commun.* 2015;6:7264.

34. Glinka Y, and Prud'homme GJ. Neuropilin-1 is a receptor for transforming growth factor beta-1, activates its latent form, and promotes regulatory T cell activity. *J Leukoc Biol.* 2008;84(1):302-310.

35. Nolte M, and Margadant C. Controlling Immunity and Inflammation through Integrin-Dependent Regulation of TGF-beta. *Trends Cell Biol.* 2020;30(1):49-59.

36. Pan L, et al. Legumain Is an Endogenous Modulator of Integrin alphavbeta3 Triggering Vascular Degeneration, Dissection, and Rupture. *Circulation.* 2022;145(9):659-674.

37. Shen YH, et al. Aortic Aneurysms and Dissections Series: Part II: Dynamic Signaling Responses in Aortic Aneurysms and Dissections. *Arterioscler Thromb Vasc Biol.* 2020;40(4):e78-e86.

38. Habashi JP, et al. Losartan, an AT1 antagonist, prevents aortic aneurysm in a mouse model of Marfan syndrome. *Science.* 2006;312(5770):117-121.

39. Gallo EM, et al. Angiotensin II-dependent TGF-beta signaling contributes to Loeys-Dietz syndrome vascular pathogenesis. *J Clin Invest.* 2014;124(1):448-460.

40. Mallat Z, et al. The Pathogenic Transforming Growth Factor-beta Overdrive

Hypothesis in Aortic Aneurysms and Dissections: A Mirage? *Circ Res.* 2017;120(11):1718-1720.

41. Daugherty A, et al. Transforming Growth Factor-beta in Thoracic Aortic Aneurysms: Good, Bad, or Irrelevant? *J Am Heart Assoc.* 2017;6(1).

42. Zhou D, et al. hiPSC Modeling of Lineage-Specific Smooth Muscle Cell Defects Caused by TGFBR1(A230T) Variant, and Its Therapeutic Implications for Loeys-Dietz Syndrome. *Circulation.* 2021;144(14):1145-1159.

43. Morrell CN, et al. Platelet olfactory receptor activation limits platelet reactivity and growth of aortic aneurysms. *J Clin Invest.* 2022;132(9).

44. Frutkin AD, et al. TGF-[beta]1 limits plaque growth, stabilizes plaque structure, and prevents aortic dilation in apolipoprotein E-null mice. *Arterioscler Thromb Vasc Biol.* 2009;29(9):1251-1257.

45. Bai H, et al. A novel intramural TGF beta 1 hydrogel delivery method to decrease murine abdominal aortic aneurysm and rat aortic pseudoaneurysm formation and progression. *Biomed Pharmacother.* 2021;137:111296.

46. Kojima Y, et al. Proefferocytic Therapy Promotes Transforming Growth Factor-beta Signaling and Prevents Aneurysm Formation. *Circulation.* 2018;137(7):750-753.

47. Inamoto S, et al. TGFBR2 mutations alter smooth muscle cell phenotype and predispose to thoracic aortic aneurysms and dissections. *Cardiovasc Res.* 2010;88(3):520-529.

48. Sood R, et al. Role of RUNX1 in hematological malignancies. *Blood.*

2017;129(15):2070-2082.

49. List A, et al. Lenalidomide in the myelodysplastic syndrome with chromosome 5q deletion. *N Engl J Med.* 2006;355(14):1456-1465.

50. Palumbo A, et al. Continuous lenalidomide treatment for newly diagnosed multiple myeloma. *N Engl J Med.* 2012;366(19):1759-1769.

51. Patel KK, et al. Safety and Efficacy of Combination Maintenance Therapy with Ixazomib and Lenalidomide in Patients with Posttransplant Myeloma. *Clin Cancer Res.* 2022;28(7):1277-1284.

52. Sawada H, et al. Ultrasound Monitoring of Descending Aortic Aneurysms and Dissections in Mice. *Arterioscler Thromb Vasc Biol.* 2020;40(10):2557-2559.

53. Sawada H, et al. Twenty Years of Studying AngII (Angiotensin II)-Induced Abdominal Aortic Pathologies in Mice: Continuing Questions and Challenges to Provide Insight Into the Human Disease. *Arterioscler Thromb Vasc Biol.* 2022;42(3):277-288.

54. Xie W, et al. Single-Cell RNA Sequencing and Assay for Transposase-Accessible Chromatin Using Sequencing Reveals Cellular and Molecular Dynamics of Aortic Aging in Mice. *Arterioscler Thromb Vasc Biol.* 2022;42(2):156-171.

55. Munshaw S, et al. Thymosin beta4 protects against aortic aneurysm via endocytic regulation of growth factor signaling. *J Clin Invest.* 2021;131(10).

56. Luo W, et al. Critical Role of Cytosolic DNA and Its Sensing Adaptor STING in Aortic Degeneration, Dissection, and Rupture. *Circulation.* 2020;141(1):42-

66.

57. Hiromi T, et al. Excessive EP4 Signaling in Smooth Muscle Cells Induces Abdominal Aortic Aneurysm by Amplifying Inflammation. *Arterioscler Thromb Vasc Biol.* 2020;40(6):1559-1573.

58. Li Z, et al. Runx2 (Runt-Related Transcription Factor 2)-Mediated Microcalcification Is a Novel Pathological Characteristic and Potential Mediator of Abdominal Aortic Aneurysm. *Arterioscler Thromb Vasc Biol.* 2020;40(5):1352-1369.

59. Hadi T, et al. Macrophage-derived netrin-1 promotes abdominal aortic aneurysm formation by activating MMP3 in vascular smooth muscle cells. *Nat Commun.* 2018;9(1):5022.

60. Qian W, et al. Microskeletal stiffness promotes aortic aneurysm by sustaining pathological vascular smooth muscle cell mechanosensation via Piezo1. *Nat Commun.* 2022;13(1):512.

61. Li G, et al. Chronic mTOR activation induces a degradative smooth muscle cell phenotype. *J Clin Invest.* 2020;130(3):1233-1251.

62. Nguyen NUN, et al. A calcineurin-Hoxb13 axis regulates growth mode of mammalian cardiomyocytes. *Nature.* 2020;582(7811):271-276.

63. Zhao G, et al. BAF60c prevents abdominal aortic aneurysm formation through epigenetic control of vascular smooth muscle cell homeostasis. *J Clin Invest.* 2022;132(21).

64. Sun LY, et al. Nuclear Receptor NR1D1 Regulates Abdominal Aortic Aneurysm

Development by Targeting the Mitochondrial Tricarboxylic Acid Cycle Enzyme Aconitase-2. *Circulation.* 2022;146(21):1591-1609.

65. Malhotra R, et al. HDAC9 is implicated in atherosclerotic aortic calcification and affects vascular smooth muscle cell phenotype. *Nat Genet.* 2019;51(11):1580-1587.

Figures and Figure legends

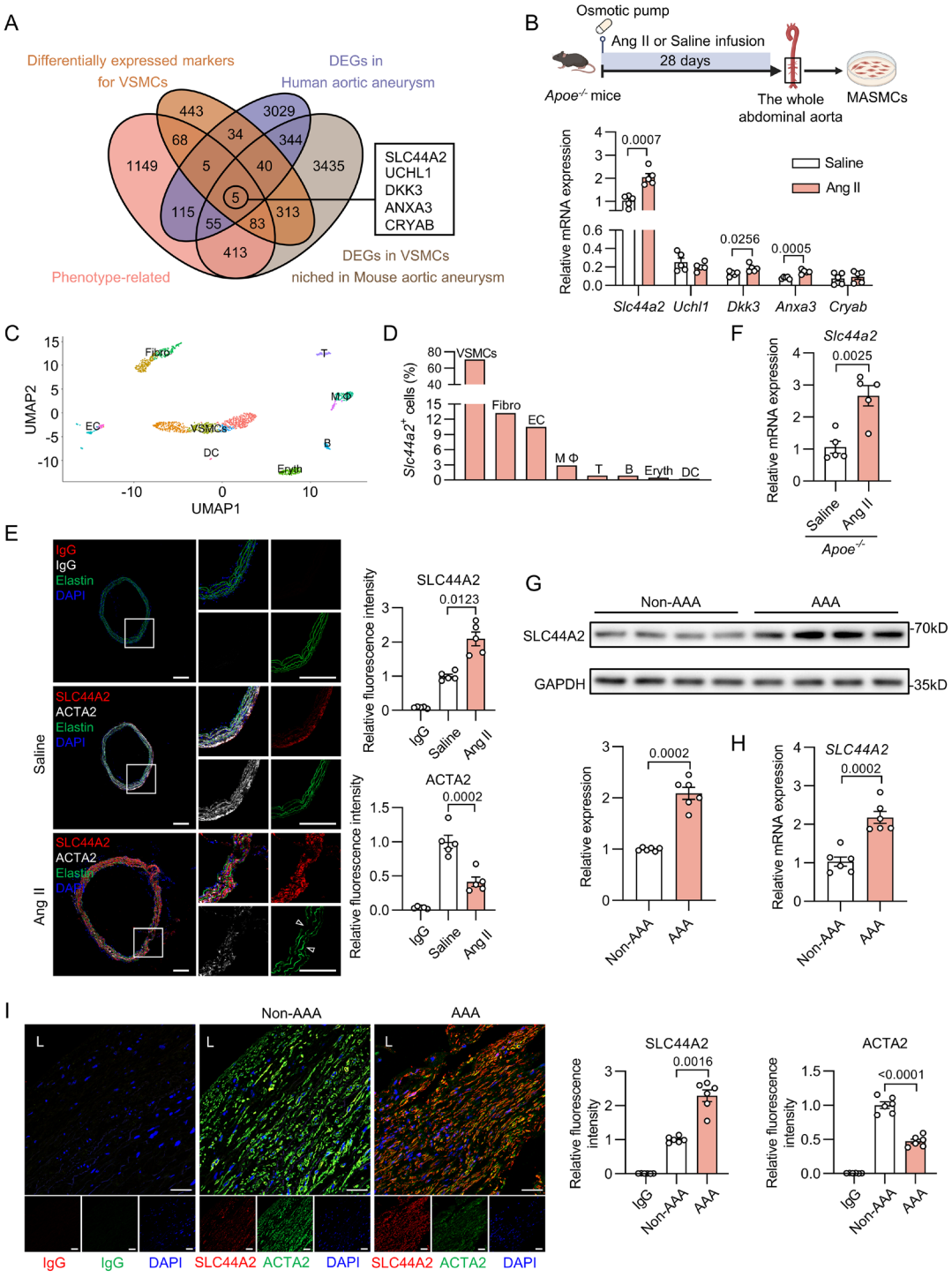

Figure 1. The aortic SLC44A2 expression is elevated in aortic aneurysm.
(**A**) Venn diagram showing the overlap between VSMCs phenotype-related genes, differentially expressed markers for VSMCs, DEGs in Human aortic aneurysm (GSE47472), and DEGs in VSMCs niched in Mouse aortic aneurysm (GSE186865). (**B**) MASMCs were isolated from the whole abdominal aortas of saline- or Ang II-infused mice. The mRNA levels of *Slc44a2*, *Uchl1*, *Dkk3*, *Anxa3*, and *Cryab* were

detected by qRT-PCR. n = 5. (**C**) Uniform Manifold Approximation and Projection (UMAP) visualization of single cells from abdominal aortic tissue of mice (GSE152583). Cells were partitioned into eight major lineages. VSMCs, vascular smooth muscle cells; Fibro, fibroblasts; EC, endothelial cells; MΦ, macrophages; T, T cells; B, B cells; Eryth, erythrocytes; DC, dendritic cells. (**D**) *Slc44a2* expression amongst distinct cellular populations. (**E** and **F**) *Apoe*$^{-/-}$ mice were infused with saline or Ang II for 28 days. (**E**) Immunofluorescence staining for SLC44A2 (red), ACTA2 (white), and DAPI (blue) in the suprarenal abdominal aorta. Elastic fibers are green (autofluorescence). Arrowheads indicate elastin breaks. IgG was used as the isotype control. Scale bar, 200 μm. n = 5. (**F**) *Slc44a2* mRNA level in aorta. n = 5. (**G**) Western blot analysis of SLC44A2 expression in the aorta from Non-AAA groups and AAA patients. n = 6. (**H**) *SLC44A2* mRNA level in the aorta from Non-AAA groups and AAA patients. n = 6. (**I**) Immunofluorescence staining for SLC44A2 (red), ACTA2 (green), and DAPI (blue) in the aortic media of Non-AAA groups and AAA patients. IgG was used as the isotype control. L, lumen. Scale bar, 40 μm. n = 6. **B**, **F**, and **H**, unpaired two-tailed *t*-test; **E**, Welch's ANOVA or one-way ANOVA; **G**, Welch's *t* test; **I**, Welch's ANOVA.

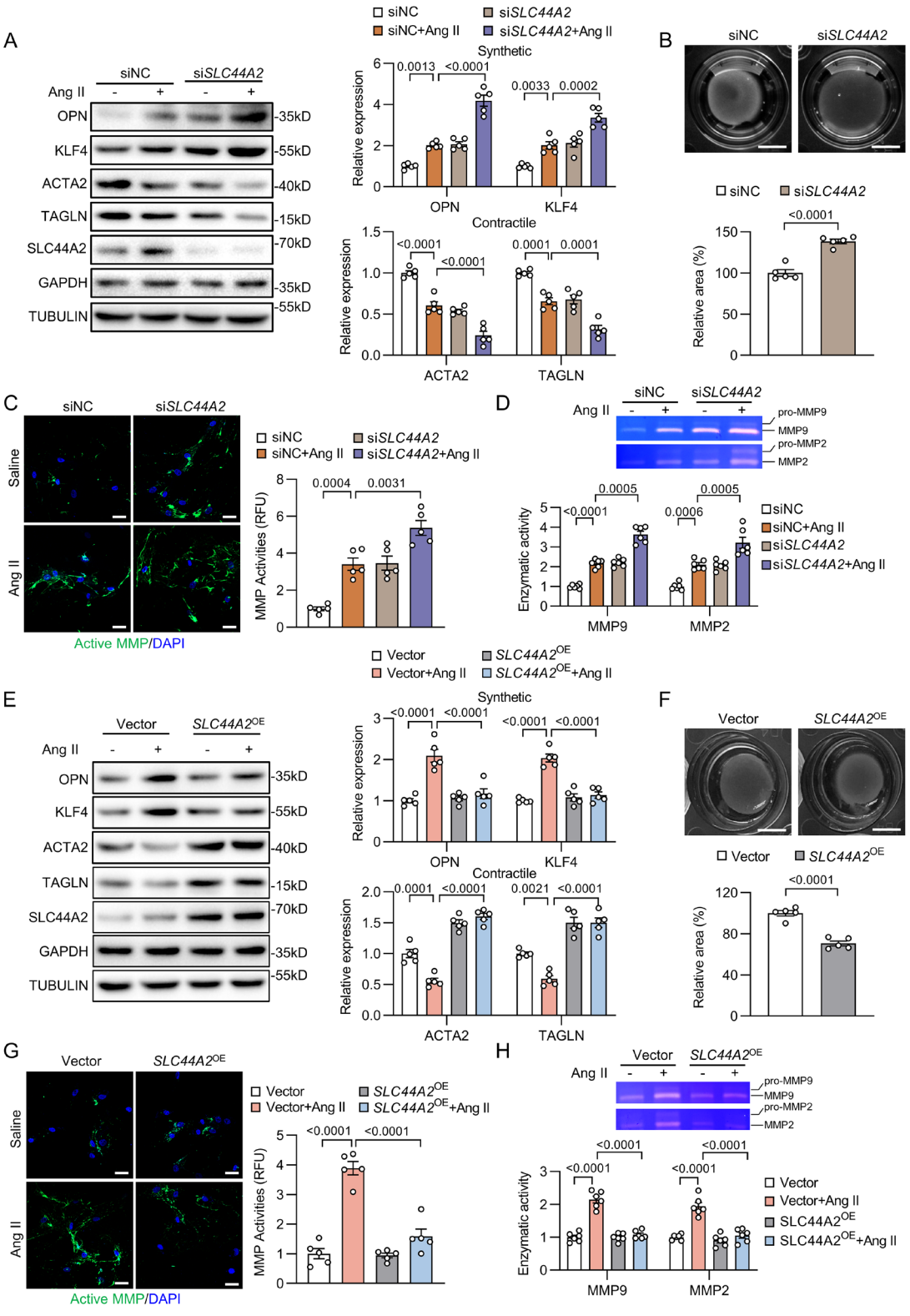

Figure 2. SLC44A2 maintains the contractile phenotype of VSMCs.

(**A-D**) HASMCs were transfected with siRNA against SLC44A2 (si*SLC44A2*) or negative control (siNC), and then treated with Ang II (1 μM, 24 hours). (**A**) The synthetic and contractile markers were detected by Western blotting. n = 5. (**B**) Contraction of HASMCs grown in collagen discs was assessed and quantified by gel

area. Scale bar, 5 mm. n = 5. (**C**) Immunofluorescence images of in situ zymography (DQ gelatin) in HASMCs. MMP activity was quantified by immunofluorescence intensity. RFU, relative fluorescence units. Scale bar, 40 μm. n = 5. (**D**) The activity of MMP2 and MMP9 in culture medium was measured by gel zymography. n = 6. (**E-H**) HASMCs were infected with lentivirus containing vector or SLC44A2 encoding plasmids to overexpress SLC44A2 (*SLC44A2*^{OE}), and then treated with Ang II (1 μM, 24 hours). (**E**) The synthetic and contractile markers were detected by Western blotting. n = 5. (**F**) Contraction of HASMCs grown in collagen discs was assessed and quantified by gel area. Scale bar, 5 mm. n = 5. (**G**) Immunofluorescence images of in situ zymography (DQ gelatin) in HASMCs. MMP activity was quantified by immunofluorescence intensity. RFU, relative fluorescence units. Scale bar, 40 μm. n = 5. (**H**) The activity of MMP2 and MMP9 in culture medium was measured by gel zymography. n = 6. **A**, **C**, **E**, **G**, and **H** one-way ANOVA; **B** and **F**, unpaired two-tailed *t*-test; **D**, Welch's ANOVA or one-way ANOVA.

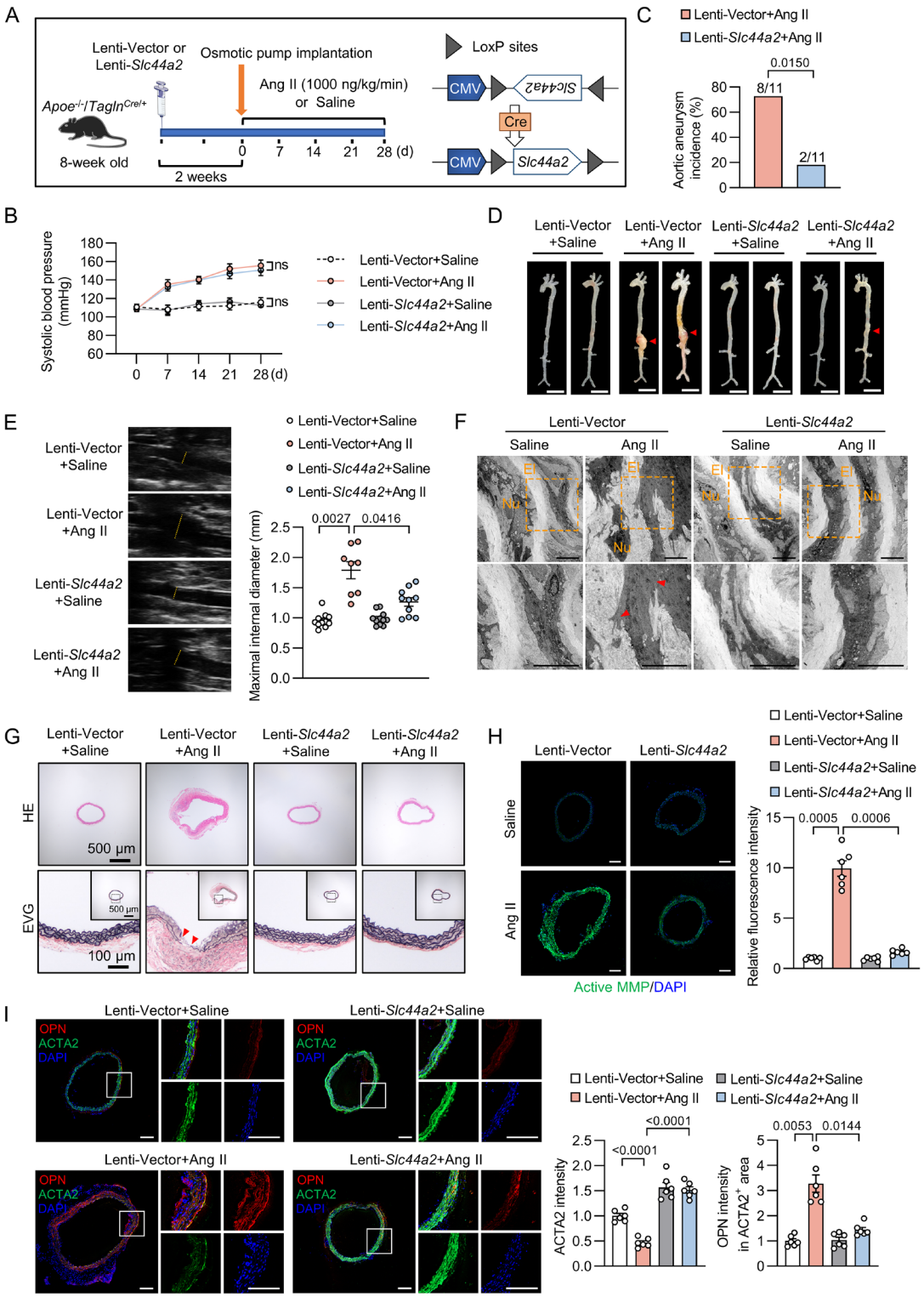

Figure 3. VSMCs overexpression of SLC44A2 moderates aortic aneurysm in Ang II-infused *Apoe*$^{-/-}$ mice.

(**A**) Eight-week-old male *Apoe*$^{-/-}$/*Tagln*$^{Cre/+}$ mice were intravenously injected with lentivirus containing control vector or reverse Slc44a2 sequence with two LoxP sites. After 2 weeks, osmotic pumps were implanted subcutaneously to infuse saline or Ang II (1000 ng/kg/min) for 28 days. (**B**) The systolic blood pressure at 0, 7, 14, 21, and 28

days after osmotic pumps implantation. n = 8-11. ns, no significance. (**C**) The incidence of aortic aneurysm in Ang II-infused mice. n = 11. (**D**) Representative morphology of aortas from saline- or Ang II-infused mice. Scale bar, 5 mm. n = 11. (**E**) Ultrasound images and inner diameter quantification of the suprarenal abdominal aorta. n= 8-11. (**F**) Electron microscopic images of the suprarenal abdominal aorta. Red arrowheads indicate elastin breaks. El, elastin; Nu, nucleus. Scale bar, 5 μm. n = 3. (**G**) Hematoxylin and eosin (HE) and elastic Verhoeff-Van Gieson (EVG) staining of the suprarenal abdominal aorta. Red arrowheads indicate elastin breaks. n = 6. (**H**) Immunofluorescence images of in situ zymography (DQ gelatin, green) in the suprarenal abdominal aorta. Scale bar, 200 μm. n = 6. (**I**) Immunofluorescence staining for OPN (red), ACTA2 (green), and DAPI (blue) in the suprarenal abdominal aorta. Scale bar, 200 μm. n = 6. **B**, two-way ANOVA with mixed-effects; **C**, Fisher's exact test; **E** and **H**, Welch’s ANOVA; **I**, one-way ANOVA or Welch’s ANOVA.

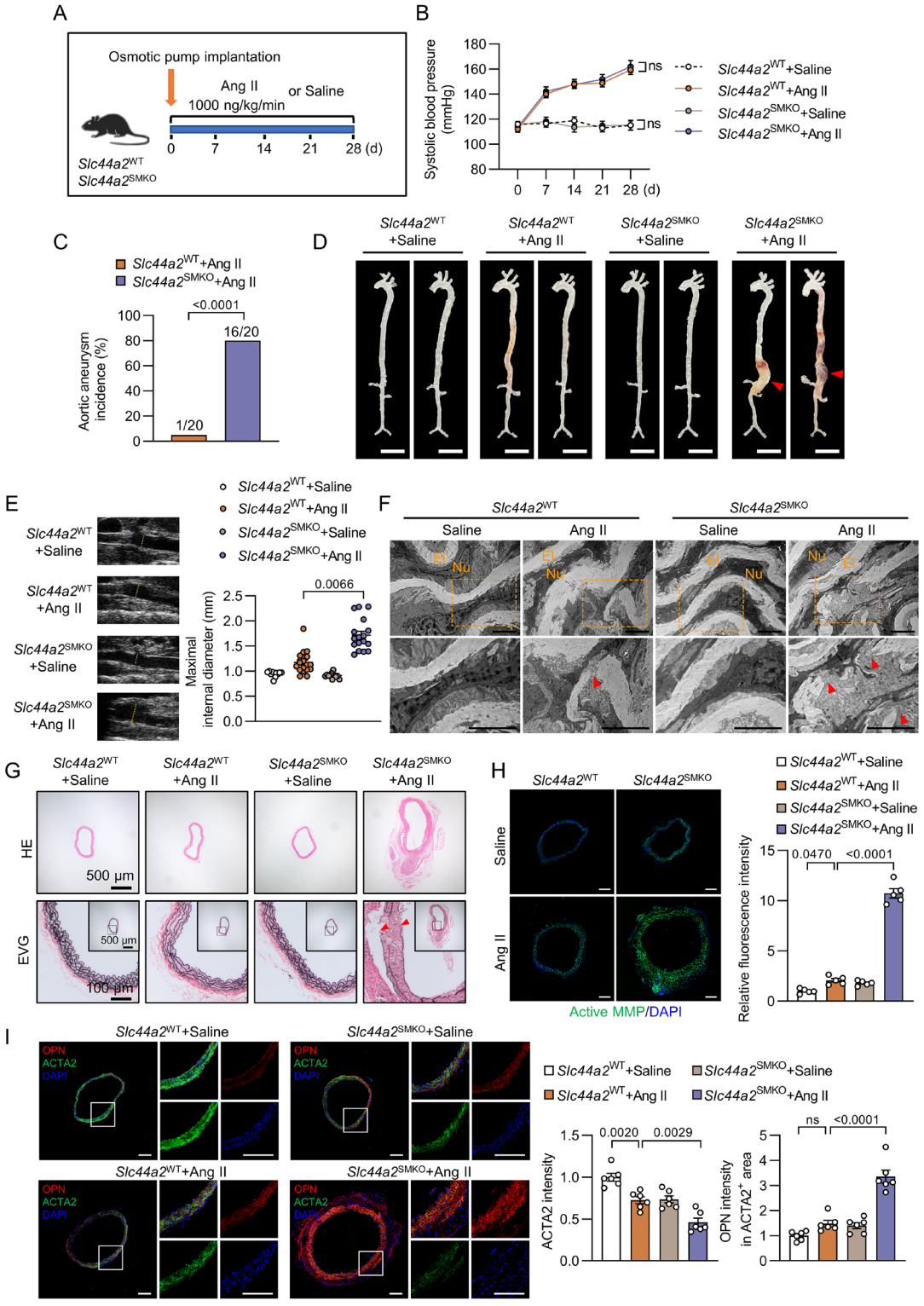

Figure 4. VSMCs knockout of SLC44A2 aggravates aortic aneurysm in Ang II-infused mice.

(**A**) Eight- to ten-week-old male *Slc44a2*^{WT} and *Slc44a2*^{SMKO} mice were infused with saline or Ang II (1000 ng/kg/min) for 28 days by osmotic pumps. (**B**) The systolic blood pressure of *Slc44a2*^{WT} and *Slc44a2*^{SMKO} mice at 0, 7, 14, 21, and 28 days after osmotic pumps implantation. n = 11-20. ns, no significance. (**C**) The incidence of aortic

aneurysm in Ang II-infused mice. n = 20. (**D**) Representative morphology of aortas from saline- or Ang II-infused mice. Scale bar, 5 mm. n = 11-20. (**E**) Ultrasound images and inner diameter quantification of the suprarenal abdominal aorta. n= 11-20. (**F**) Electron microscopic images of the suprarenal abdominal aorta. Red arrowheads indicate elastin breaks. El, elastin; Nu, nucleus. Scale bar, 5 μm. n = 3. (**G**) HE and EVG staining of the suprarenal abdominal aorta. Red arrowheads indicate elastin breaks. n = 5. (**H**) Immunofluorescence images of in situ zymography (DQ gelatin, green) in the suprarenal abdominal aorta. Scale bar, 200 μm. n = 5. (**I**) Immunofluorescence staining for OPN (red), ACTA2 (green), and DAPI (blue) in the suprarenal abdominal aorta. Scale bar, 200 μm. n = 6. **B**, two-way ANOVA with mixed-effects; **C**, Fisher's exact test; **E**, Kruskal-Wallis test; **H** and **I**, one-way ANOVA.

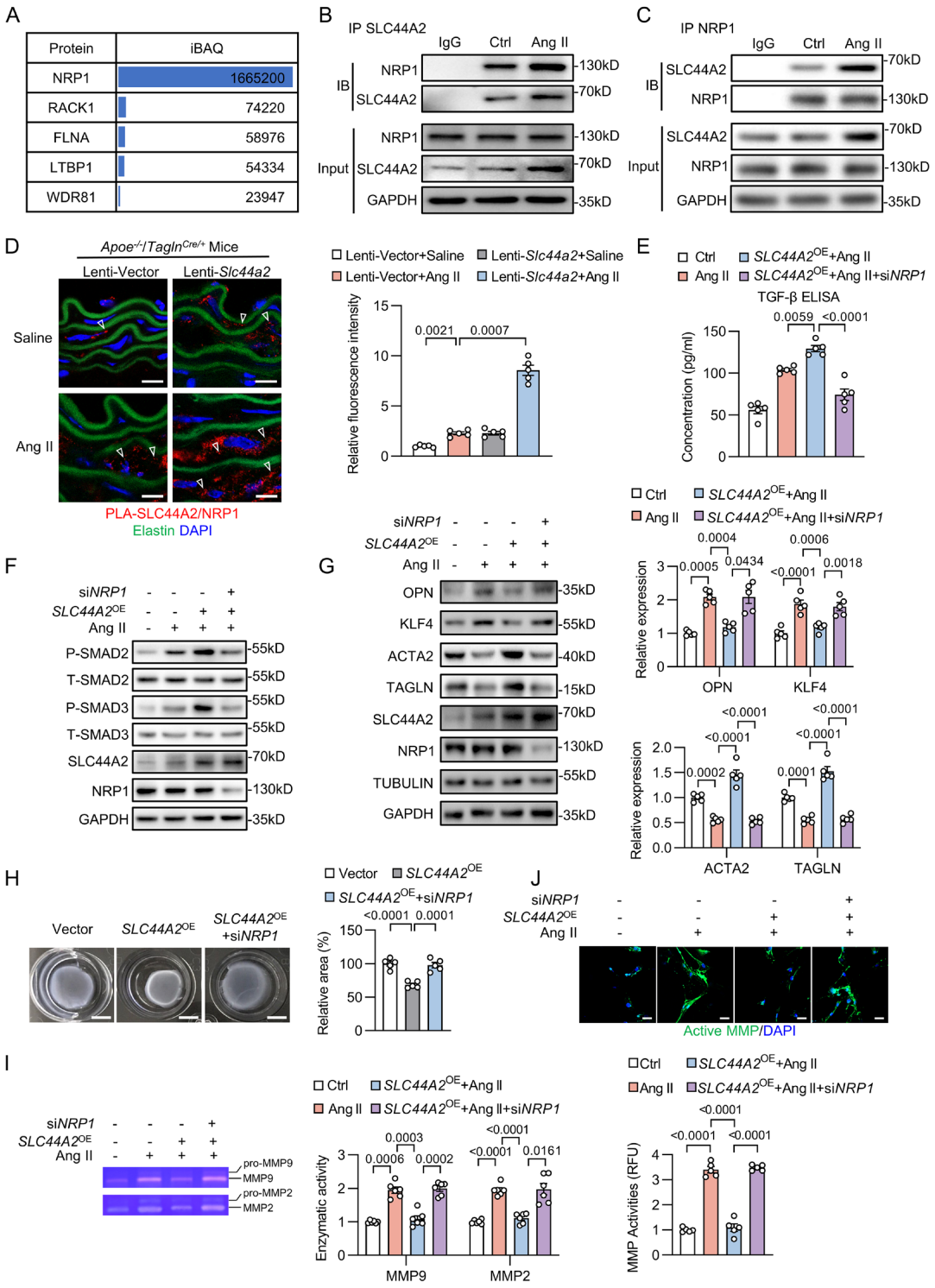

Figure 5. SLC44A2 activates TGF-β signaling to maintain the VSMCs contractile phenotype via NRP1.

(**A**) Lysates from HASMCs were immunoprecipitated with anti-SLC44A2 antibody followed by mass spectrometry analysis to identify the proteins that interact with SLC44A2. The graph showed the TGF-β signaling-related proteins. iBAQ, intensity-based absolute quantification. (**B**) HASMCs were treated with Ang II (1 μM). Lysates were immunoprecipitated with anti-SLC44A2 antibody, and blotted with anti-NRP1

and anti-SLC44A2 antibodies. n = 5. (**C**) HASMCs were treated with Ang II. Lysates were immunoprecipitated with anti-NRP1 antibody, and blotted with anti-SLC44A2 and anti-NRP1 antibodies. n = 4. (**D**) *Apoe*$^{-/-}$/*Tagln*$^{Cre/+}$ mice were intravenously injected with lentivirus containing control vector or Slc44a2. Osmotic pumps were then implanted subcutaneously to infuse saline or Ang II. The interaction of SLC44A2 with NRP1 (red dots marked by arrowheads) in suprarenal abdominal aorta was detected by proximity ligation assay (PLA). Scale bar, 10 μm. n = 5. (**E-J**) HASMCs were infected with lentivirus containing vector or SLC44A2 encoding plasmids with or without si*NRP1* transfection, then treated with Ang II. (**E**) The TGF-β levels in culture medium was measured by ELISA. n = 5. (**F**) The levels of p-SMAD2 and p-SMAD3 were detected by Western blotting. n = 4. (**G**) The levels of VSMCs synthetic and contractile markers were detected by Western blotting. n = 5. (**H**) Contraction of HASMCs grown in collagen discs was assessed and quantified by gel area. Scale bar, 5 mm. n = 5. (**I**) The activity of MMP2 and MMP9 in culture medium was measured by gel zymography. n = 6. (**J**) Immunofluorescence images of in situ zymography (DQ gelatin) in HASMCs. MMP activity was quantified by immunofluorescence intensity. Scale bar, 40 μm. n = 5. **D**, Welch's ANOVA; **E**, **H**, and **J**, one-way ANOVA**; G**, one-way ANOVA or Welch's ANOVA; **I**, Welch's ANOVA.

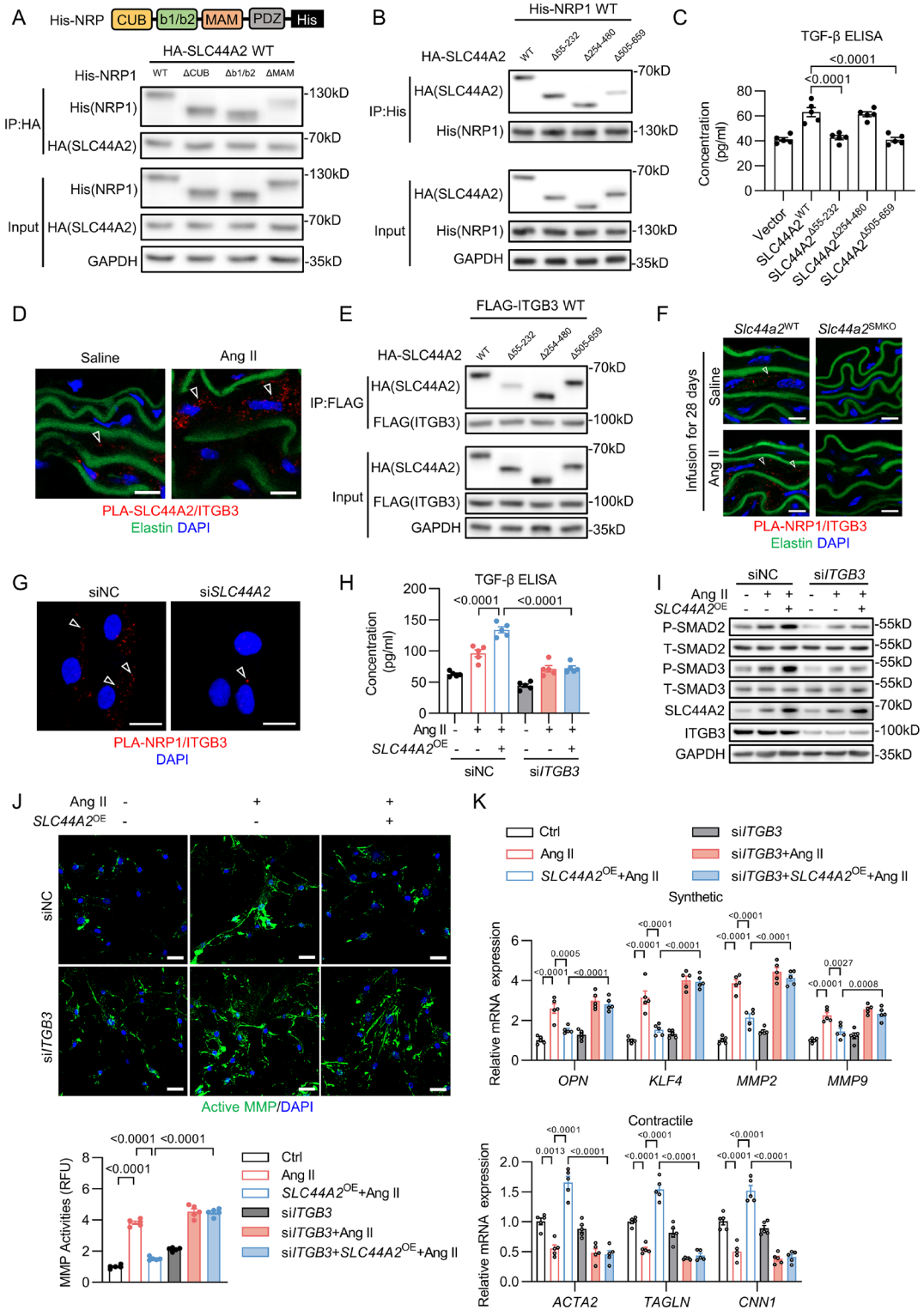

Figure 6. SLC44A2 mediates the activation of TGF-β by interacting with NRP1 and ITGB3.

(**A**) HEK293 cells were transfected with SLC44A2^{WT} and plasmids encoding NRP1^{WT}, NRP1$^{\Delta CUB}$, NRP1$^{\Delta b1/b2}$, and NRP1$^{\Delta MAM}$. Lysates were immunoprecipitated with anti-HA antibody, and blotted with anti-His and anti-HA antibodies. n = 3. (**B**) HEK293 cells were transfected with NRP1^{WT} and plasmids encoding SLC44A2^{WT}, SLC44A2$^{\Delta 55-}$

^{232}, SLC44A2$^{\Delta 254\text{-}480}$, and SLC44A2$^{\Delta 505\text{-}659}$. Lysates were immunoprecipitated with anti-His antibody, and blotted with anti-His and anti-HA antibodies. n = 3. (**C**) MASMCs from *Slc44a2*^{KO} mice were infected with lentivirus containing vector or SLC44A2 encoding plasmids. The TGF-β level in culture medium was measured by ELISA. n = 5. (**D**) The interaction of SLC44A2 with ITGB3 in suprarenal abdominal aorta from *Apoe*$^{-/-}$ mice was detected by PLA. Scale bar, 10 μm. n = 3. (**E**) HEK293 cells were transfected with ITGB3^{WT} and plasmids encoding SLC44A2^{WT}, SLC44A2$^{\Delta 55\text{-}232}$, SLC44A2$^{\Delta 254\text{-}480}$, and SLC44A2$^{\Delta 505\text{-}659}$. Lysates were immunoprecipitated with anti-FLAG antibody, and blotted with anti-FLAG and anti-HA antibodies. n = 3. (**F**) The interaction of NRP1 with ITGB3 in suprarenal abdominal aorta from *Slc44a2*^{WT} and *Slc44a2*^{SMKO} mice was detected by PLA. Scale bar, 10 μm. n = 5. (**G**) The interaction of NRP1 with ITGB3 was detected in si*SLC44A2* transfected HASMCs by PLA. Scale bar, 20 μm. n = 3. (**H-K**) HASMCs were infected with lentivirus containing vector or SLC44A2 encoding plasmids with or without si*ITGB3* transfection, and then treated with Ang II. (**H**) The TGF-β level in culture medium was measured by ELISA. n = 5. (**I**) p-SMAD2 and p-SMAD3 levels were detected by Western blotting. n = 3. (**J**) Immunofluorescence images and quantification of in situ zymography (DQ gelatin). Scale bar, 40 μm. n = 5. (**K**) VSMCs synthetic and contractile markers were detected by qRT-PCR. n = 5. **C**, **H**, **J**, and **K**, one-way ANOVA.

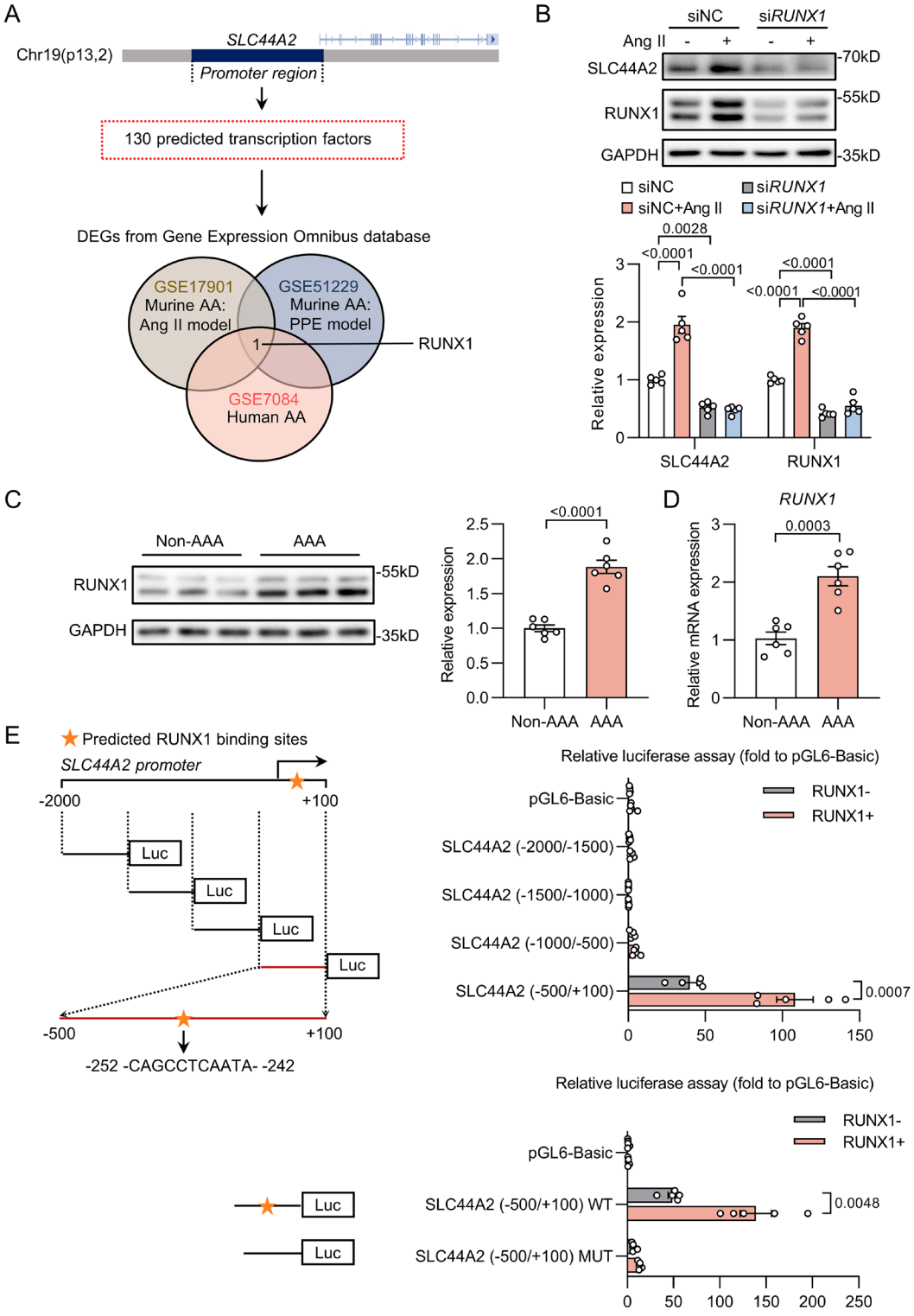

Figure 7. The transcription of SLC44A2 is regulated by RUNX1.

(**A**) Prediction of *SLC44A2* promoter-binding transcription factors by JASPAR and with the upstream 2000 bp to downstream 100 bp region of *SLC44A2* gene transcription initiation site set as the promoter region. Venn diagram of DEGs in murine (GSE17901 and GSE51229) and human (GSE7084) aortic aneurysm samples relative to normal controls from Gene Expression Omnibus database. AA, aortic aneurysm; PPE, porcine

pancreatic elastase. (**B**) HASMCs were transfected with si*RUNX1* or siNC, and then treated with Ang II (1 μM, 24 hours). The levels of SLC44A2 and RUNX1 were detected by Western blotting. n = 5. (**C**) Western blot analysis of RUNX1 in the aortas of Non-AAA and AAA subjects. n = 6. (**D**) *RUNX1* mRNA level in the aortas of Non-AAA and AAA subjects was detected by qRT-PCR. n = 6. (**E**) Relative luciferase activity in HEK293 cells of luciferase reporter constructs containing *SLC44A2* promoter truncations or its mutants transfected along with pRL-TK (internal control plasmid) followed by transfection with RUNX1 encoding plasmid. n = 5. **B**, one-way ANOVA; **C** and **D**, unpaired two-tailed *t*-test; **E**, unpaired two-tailed *t*-test or Welch's *t* test.

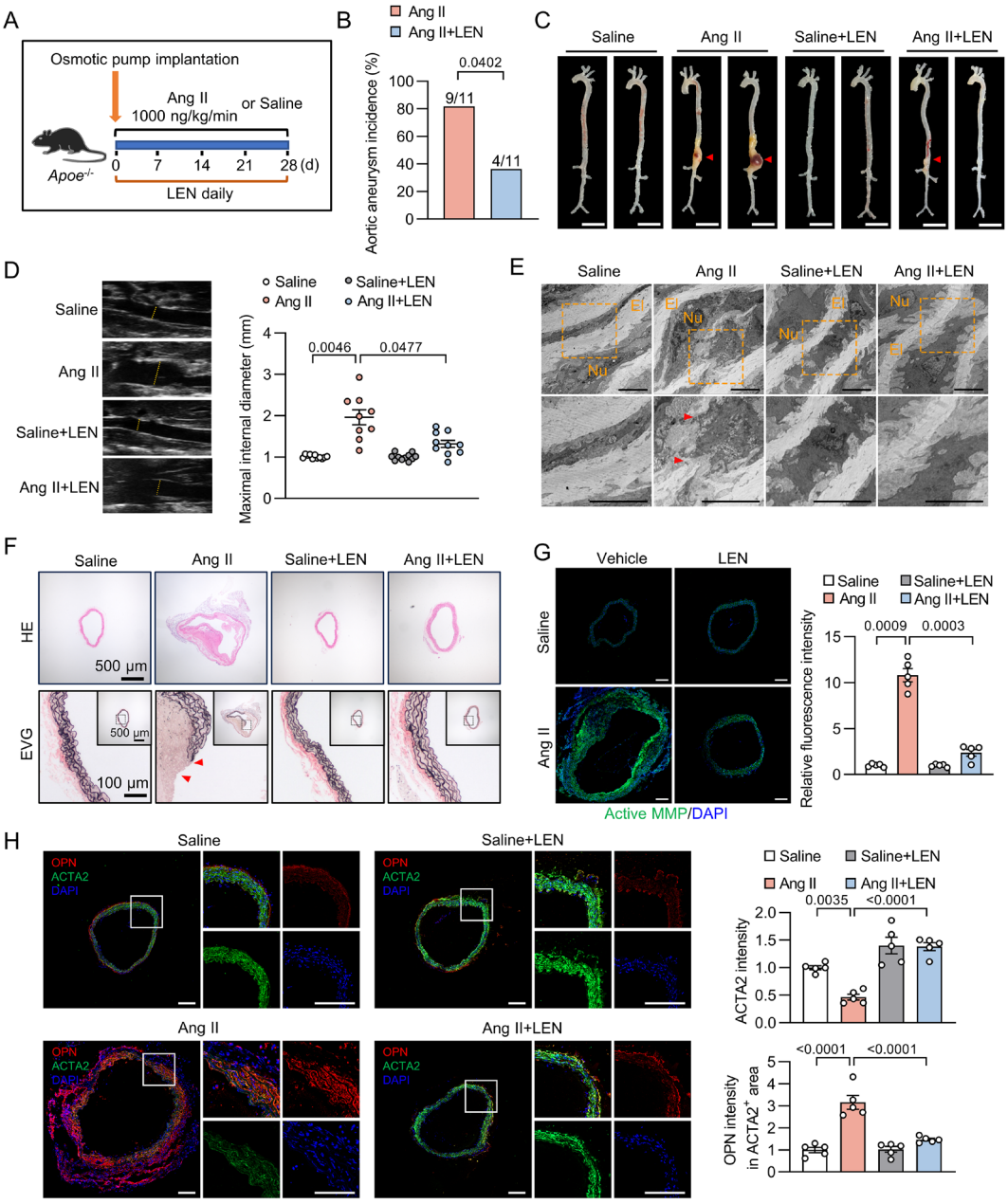

Figure 8. Administration of LEN relieves aortic aneurysm in mice.

(**A**) Eight- to ten-week-old male *Apoe*$^{-/-}$ mice were implanted subcutaneously with osmotic pumps to infuse saline or Ang II (1000 ng/kg/min) with or without intragastric administration of LEN (20 mg/kg/day) for 28 days. (**B**) The incidence of aortic aneurysm in Ang II-infused *Apoe*$^{-/-}$ mice administrated with vehicle or LEN. n = 11. (**C**) Representative morphology of aortas from Ang II-infused *Apoe*$^{-/-}$ mice administrated with vehicle or LEN. Scale bar, 5 mm. n = 11. (**D**) Ultrasound images and inner diameter quantification of the suprarenal abdominal aorta. n = 9-11. (**E**) Electron microscopic images of the suprarenal abdominal aorta. Red arrowheads indicate elastin breaks. El, elastin; Nu, nucleus. Scale bar, 5 μm. n = 3. (**F**) HE and EVG staining of the suprarenal abdominal aorta. Red arrowheads indicate elastin breaks. n = 5. (**G**) Immunofluorescence images of in situ zymography (DQ gelatin, green) in the suprarenal abdominal aorta. Scale bar, 200 μm. n = 5. (**H**) Immunofluorescence staining for OPN (red), ACTA2 (green), and DAPI (blue) in the suprarenal abdominal aorta. Scale bar, 200 μm. n = 5. **B**, Fisher's exact test; **D** and **G**, Welch's ANOVA; **H**, one-way ANOVA.

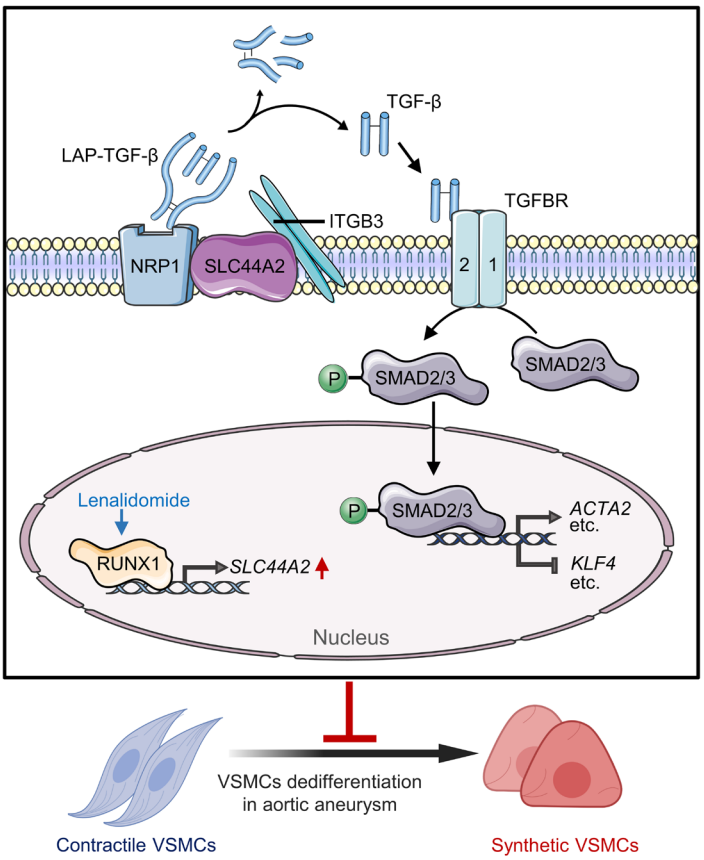

Figure 9. Proposed model for SLC44A2 as a therapeutic target in aortic aneurysm. Lenalidomide promotes RUNX1-mediated transcription of SLC44A2. The upregulated SLC44A2 acts as a scaffolding protein to interact with NRP1 and ITGB3 to activate TGF-β/SMAD signaling, further promoting the expression of VSMCs contractile genes and inhibiting the expression of VSMCs synthetic genes to restrain the VSMCs phenotypic switching in aortic aneurysm.